La Chimica è materia,

ma anche immaginazione,

che dà vita all'invisibile agli occhi.

La Chimica è vita e spazio circostante,

è il vuoto e ciò che lo riempie.

La Chimica è l'inizio e l'equilibrio,

la domanda e la risposta,

la magia, la follia.

UNIVERSITA' DEGLI STUDI DI SALERNO

Facoltà di Scienze MM.FF.NN.

Dipartimento di Chimica e Biologia

Dottorato di Ricerca in Chimica – XII CICLO

Tesi di Dottorato

Transport properties of drug precursor molecules in nanoporous polymers.

Relatore:
Prof. Vincenzo Venditto

Candidata:
Marianna Loria
Mat. 8880700110

Coordinatore
Prof. Gaetano Guerra

Anno Accademico 2012/2013

Summary

Abstract

This PhD thesis is framed in the European project CUSTOM, which aims to develop a small size device able to detect drug precursors molecules in the air, even when they are just in traces. The project is part of the European strategies to fight the illegal drug trafficking, that is a serious problem experienced in all countries worldwide. Recently, in fact, drug traffickers smuggle drug precursor molecules, that is molecules that are converted into the final product through chemical processes, once arrived in the country of destination. For this reason many efforts are making to detect the presence of precursors in very low concentrations using dedicated sensors. The low concentration of these kind of molecules requires that the sampling techniques concentrate as much as possible the target analytes. For this purpose, syndiotactic polystyrene (sPS), a cheap and commercial thermoplastic polymer, can be a good choice: it can be achieved in highly porous crystalline morphologies (aerogels) able to maximize molecules sorption and desorption kinetics thanks to their high surface area[1]. High-porosity sPS aerogels can be obtained by supercritical CO_2 extraction of the solvent present in sPS physical gels (gels in which the junctions between polymer chains consist of crystalline regions).

Furthermore, sPS crystalline aerogels can be achieved in two different nanoporous crystal forms, delta (δ) and epsilon (ε). These two phases present well-defined empty spaces distribute into the crystal lattice as cavities (δ form) or channels (ε form). Both these two crystalline forms are able to rapidly absorb volatile organic compounds (VOCs), mainly halogenated or aromatic hydrocarbons, from water and air also when present at very low concentrations[2]. This polymer, combined with a suitable detection system for these precursor molecules, could be a winning choice for the purposes of the CUSTOM project.

Within the project, our tasks and objectives are to evaluate the capacity and the effectiveness of the polymer to absorb some target drug precursors, to validate the air sampling module which will be implemented in the device and, finally, to establish if and how the presence of some common pollutants in the air could affect the sorption of the selected precursors.

Chapter 1
Introduction

This PhD thesis is framed and funded by the European research project CUSTOM, acronym of “Drugs and Precursors Sensing by Complementing Low Cost Multiple Techniques”, set up by different companies and scientific research centres under the Seventh Framework Programme of European Union. This research project aims to develop a portable device capable of detecting traces of chemical drug precursors used in the manufacture of the most dangerous drugs on the International market. The device will consist of two detectors (Laser photo-acoustic spectroscopy or LPAS and Light Emitting diode – Induced Fluorescence or LED-IF), a control board and an air sampling part. The core of this latter part is a preconcentrator unit (PCU), based on porous materials necessary to trap and concentrate as much as possible the drug precursors from the air, where they are difficult to detect due to their very low concentration in the vapour phase. Moreover, there is also the need to detect these precursors in a short time because this device is thought to be used in different scenarios such as ports, airports, railway stations, customs and so on.

The partners involved in the CUSTOM project and their

respective tasks are:

1. SELEX-ES (Italy), a new brand of FINMECCANICA holding, world leader of Defence Systems and Sensors and Air Traffic Management and Control. It is in charge of the management of the project, of the definition of sensor and control board requirements and of the device integration and testing.
2. GASERA Ltd. (Finland), a university based spin-off company developing novel technologies for the measurements of gas concentrations, is involved in the architecture of the sensor node.
3. University of Turku (Finland), where its Laboratory of Optics and Spectroscopy is focused on theory and applications of the photoacoustic trace gas detection and on quantum optics, so it takes part in the design of the LPAS sensor chamber.
4. Tecnalia (Spain), a private technological centre providing research and technological development services to institutions and productive industries, here engaged with realization of LED-IF sensor.
5. III-V Lab (France), a private R&D organisation focused on research in the field of III-V semiconductors. Its task will be the realization of the quantum cascade laser (QCL) for the LPAS

sensor.

6. CNR IBP (Italy), the Institute of Protein Biochemistry of the Italian National Research Council that studies proteins and enzymes using the most advanced approaches and techniques, and that in the project deals with fluorescence optochip sensing.
7. ENEA (Italy), the Italian National Agency for New Technologies, Energy and the Environment, a public organisation operating in the fields of energy, environment and new technologies to support competitiveness and sustainable development. Here it is concerned with the design and electronics of air traces sampling part, in particular of the PCU.
8. INSTM (Italy), the National Institute for the Science and Technology of Materials, a consortium of universities that collects more than 44 Italian institutes. For the execution of this project, the groups representing INSTM are the University of Modena and Reggio Emilia, involved in the design of algorithms to create a data base software, and the University of Salerno, involved in the molecular concentrator of drug precursors from air traces.
9. Aalto University Foundation (Finland), whose Department of Micro and Nanosciences focuses in optoelectronics, photonics and microelectronics,

takes care of microelectromechanical systems (MEMS) of the LPAS sensor.

10. Direction National du Reinsegnement et des Enquêtes Douanières (France), belonging to the French Customs Administration. Its task are the identification of application scenarios and the device test in real environment.

1.1 The illegal trafficking of drugs

The problem of trafficking in illegal drugs is a serious concern that involves various Nations all over the world and many efforts have been made in the past twenty years to stem this problem.

A good way to prevent the trafficking of illegal drugs is intercept them before they are shipped to countries of destination, that is those ones in which they will be consumed. Another way to stop this trafficking is checking the route of substances used to manufacture the drug, also known as chemical precursors (or simply precursors). In fact, the traffickers recently use to smuggle the drug precursors rather than the drugs as such, because it is easier since the same type of drug can be obtained from different precursors. Moreover, a lot of time is needed to point out systems capable to intercept them, so the traffickers can act almost undisturbed and they have

enough time to change the way of smuggling until the authorities catch them up.

The chemical precursors are substances that play two essential roles in the production of illegal drugs: both as starting reagents for the production of synthetic drugs and as refining agents and solvents in the processing of plant-based materials.

In the definition of precursors are then included both substances extracted from plants such as opium poppy and coca useful in the production of heroin and cocaine, respectively, which can be easily replaced by other molecules with similar properties, and substances used in synthetic drug (like methamphetamine and ecstasy) production which are incorporated in the final product and are less easily replaceable with other molecules.

The International Narcotics Control Board (INCB) focuses its efforts on preventing the diversion of chemical precursors used in the illicit manufacture of heroin, cocaine and amphetamine-type stimulants. The official reference work for the international control of precursors is the Annex to the Article 12 of the 1988 United Nations Convention Against Illicit Traffic in Narcotic Drugs and Psycothropic Substances[3], that establishes two tables listing 23 substances frequently used in the manufacture of drugs and whose diversion to illicit purposes should be

prevented. These tables (collected in the following Table 1.1) are regularly updated to take account of developments and evolutions in the production of illegal drugs, thanks to the information shared by different countries in collaboration with the INCB. The Article 12 and the list of the 23 most common drug precursors under international control were adopted also by European legislation in 1990, even if the substances were separated in three categories[4].

Table 1.1. Lists of the 23 substances considered chemical precursors by the United Nations Convention.

Table I	Table II
Acetic anhydride	Acetone
N-Acetylanthanilic acid	Anthranilic acid
Ephedrine	Ethyl ether
Ergometrine	Hydrochloric acid
Ergotamine	Methyl ethyl ketone
Isosafrole	Phenylacetic acid
Lysegic acid	Piperidine
3,4-Methylnedioxyphenyl-2-propanone	Sulphuric acid
Norephedrine	Toluene
1-Phenyl-2-propanone	
Piperonal	
Potassium permanganate	
Pseudoephedrine	
Safrole	

Some substances in “Table I” and “Table II” are indispensable for the manufacture of synthetic drugs (amphetamine-type stimulants), such as ephedrine and pseudoephedrine for methamphetamine; 3,4-Methylnedioxyphenyl-2-propanone, isosafrole and safrole for ecstasy; 1-Phenyl-2-propanone for amphetamine and methamphetamine. Other substances of these tables,

instead, are important reagents used in the production of cocaine and heroin, such as potassium permanganate and acetic anhydride.

The substances in the column “Table I” are the less replaceable in the production of illegal drugs and those ones above mentioned are the most seized in the last years, according to the INCB[5-6]. Anyway, it is not simple for the authorities to intercept the precursors diverted by the traffickers from their legitimate purposes and licit trades. Diversion from licit trades can be done in many ways. The chemicals may be diverted with the complicity of the chemical producers, even if this is less frequent. Instead, most diversion takes place due to the ability of criminals to exploit gaps in the regulatory frameworks in place to monitor the trade in drug precursors and identify suspicious transactions. International trade in drug precursors can be exploited by traffickers through different means. Precursors can be imported legally into drug-producing countries with official import permits and subsequently diverted into neighbouring illegal drug-producing countries. In parts of the developing world, traffickers often arrange for chemicals to be shipped to countries where no viable regulatory systems exist for their control (figure 1.1).

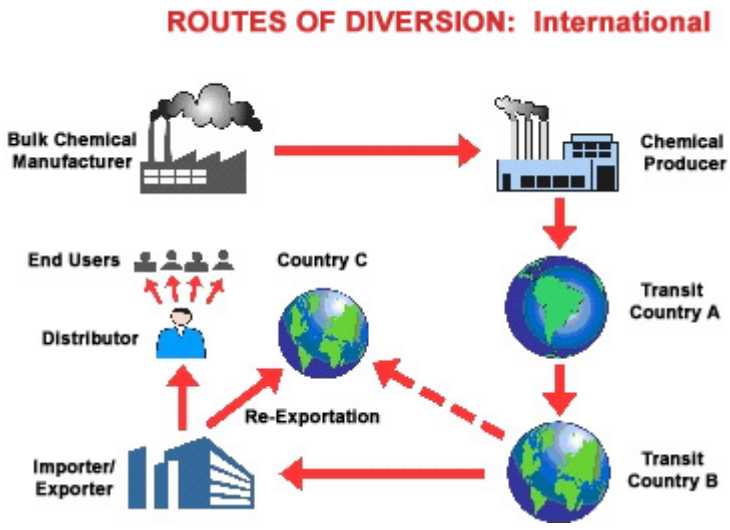

Figure 1.1 Routes of drug precursors diversion

Criminals often conceal their identity by using front-companies or by misusing the names of well-known companies. They also obtain chemicals by bribing or blackmailing the employees of legitimate companies. In some cases they disguise the destination or nature of chemical shipments by mislabelling or re-packaging controlled chemicals as unregulated materials. Traffickers also obtain precursors through theft, either from storage or during transit.

However, in the last years smuggling from third countries into drug producing countries has increased dramatically. This tactic is emerging as a key method in response to the increasing efforts of more countries to implement legislative and administrative controls to prevent diversion

from legitimate commercial trade.

1.2 CUSTOM device

The CUSTOM project rises just with the aim to avoid the illegal trafficking of the substances above mentioned and intercept their diversion into illicit uses, by designing and realizing a proper device capable to operate in different kinds of environmental conditions, different scenarios and that is a competitive apparatus. The device, in fact, will be portable to work in scenarios such as ports, airports, railway stations, customs border, where there is a large flow of people, shipments, cars, trucks, trains. It will be also capable to analyze both solid and liquid chemical precursors. Besides, the device is expected to be easy to handle and operate for dimensions, weight, data acquisition; capable of giving trusting results for targeted precursors; having low cost of production, selling, and maintenance.

CUSTOM project partners have made a selection of target chemical precursors that will be detected by the sensors of the device. In order to select the most critical precursors smuggled, only substances listed in the column “Table I” of the United Nations Convention in 1988 have been taken into account, discarding chemicals listed in the column “Table II”. Based on the major trends identified for illicit

trafficking in chemical precursors[5], on the precursors most seized in Europe and worldwide, on the objective of the CUSTOM project to reveal precursors for drugs of both vegetal and synthetic origin, the project partners proposed to develop a device for the detection of the following five chemical precursors:

1. 1-Phenyl-2-propanone (or benzyl methyl ketone)
2. Acetic anhydride
3. Safrole
4. Ephedrine
5. Potassium permanganate

Studying the devices already available on the market, the CUSTOM project aims to develop a technology which offers an appropriate detection of the target precursors and can be easily extended and adapted to other precursors detection.

Common characteristics which are also limitation of commercially existing devices are the absence of flexibility respect to the target substances and the uniqueness of the adopted sensing technology. In fact, each device is specific for a fixed number and type of target compounds, while the fight against illicit substances requires adaptive sensors because easier replaceable drug precursors can be easily found in ever changing chemical formulas produced by drug dealers. Moreover, all the commercially existing

devices are based on a single detection technique but, for the same reasons mentioned above, it would be better employing more than one detection system.

Among the different techniques already adopted in available devices, those ones selected for CUSTOM sensor device are:

- LPAS *(Laser Photo-acoustic Spectroscopy)* technique that is proven to have high sensitivity for one with respect to other techniques based on infrared spectroscopy for a high probability of detection.

- LED-IF *(Light Emitting diode – Induced Fluorescence)* infrared optochip that is a low cost, compact device that can be made very selective with respect to the various drug specimens for a low probability of false alarm.

The LPAS sensor is highly sensitive but poorly selective towards the target drug precursors molecules, so if it gives a positive answer to the presence of one of these molecules, then the LED-IF technique, more selective than the first one, will be able to say definitely whether the molecule in question is actually present or not in the analyzed sample. Furthermore, both technologies will be enhanced.

The fluorescence signal will be intensified by development of organic macromolecules sensitive to specific classes of compounds involving our target molecules. The fluorescence analysis will be based on an optochip which can incorporate an array of different fluorescent chemical proteins able to bind to the analytes. An array classes of compounds will be thus fast discriminated by one-shot measurement. Thus, the probability of detection of the LED-IF technique will be increased.

The selectivity of medium infra-red (MIR) and microelectromechanical systems (MEMS) cantilever based photoacoustic cell (PAS) techniques will be improved by adopting a high power, high stability and tunable quantum cascade laser (QCL).

Anyway, to increase the sensitivity and the selectivity of both kinds of sensors, it is necessary to concentrate the precursors. For this reason in the architecture of the CUSTOM device is designed the PCU, based on porous materials being able to host the precursors molecules. The PCU can make more selective the LPAS technique uptaking only target molecules and not the volatile organic compounds (VOCs) interfering agents, too, and can make more sensible LED-IF sensor by rising the concentration of detected molecules.

A schematic drawing of how the whole CUSTOM device will

be made is reported in figure 1.2. All the parts of the device, control board, air sampling and detectors, are included in a mechanical cover. The control board is connected to an external PC to collect and visualize measurement results.

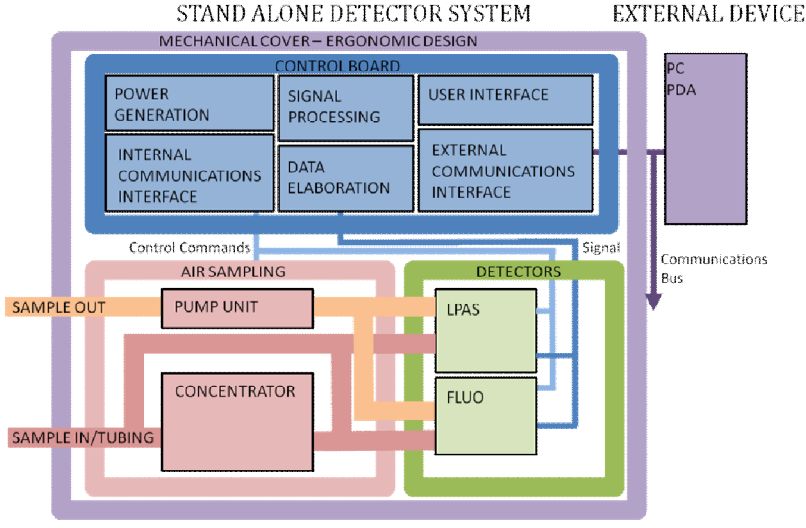

Figure 1.2 The block diagram of CUSTOM device components.

In figure 1.3, instead, is shown in more detail the block diagram of the air sampling system. An air flow is sucked by a pump from the surrounding environment and passes through the PCU. The air flow outgoing from the PCU is send to LED-IF (or FLUO) and LPAS sensors, whose response is analyzed by the control board, and then ejected to the external environment.

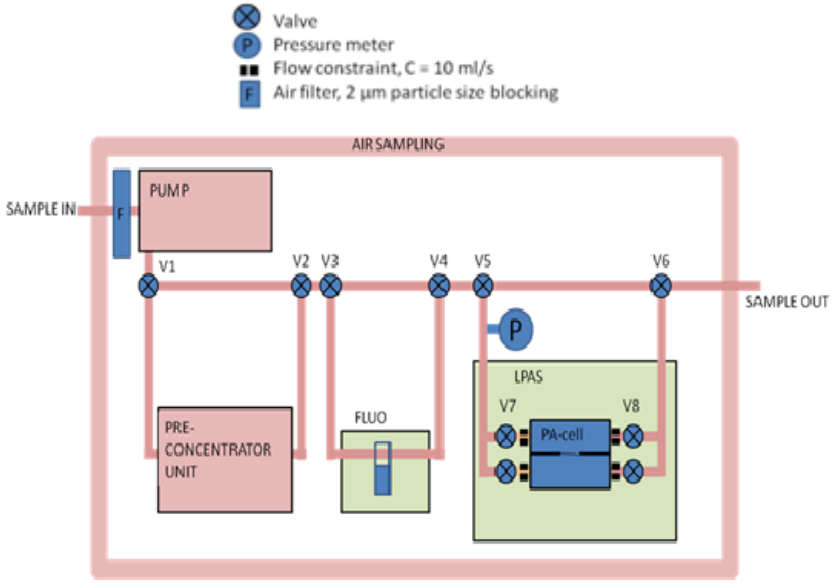

Figure 2.3 The block diagram of air sampling system.

The mechanical part of the PCU, shown in figure 1.4, is like a sort of box having some slots covered by Peltier elements to allow heating/cooling cycles, necessary to perform the sorption and desorption of the molecules in a short time. Inside these slots are placed aerogel beads of a porous polymer, the syndiotactic polystyrene (sPS), which is the concentrating material able to host the molecules in its crystalline phase and it is provided by our group. Within the CUSTOM project, our tasks are not only the production, characterization and supply of this polymer, but also the demonstration of its efficacy in concentrating target molecules and the validation of the PCU, as it will be implemented in the device, through measurements of

sorption and desorption of targeted precursors.

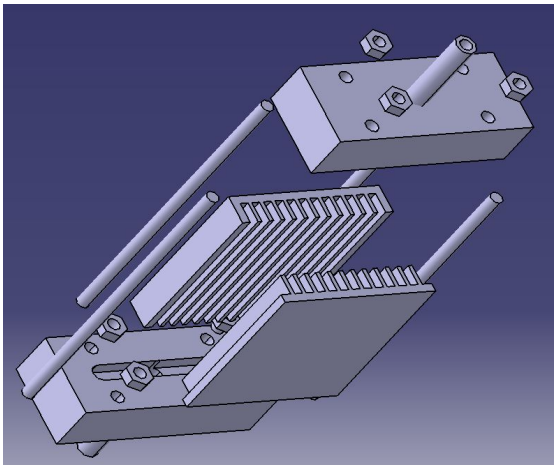

Figure 3.4 The mechanical part of the preconcentrator unit (PCU).

1.3 Concentrating porous materials

In the analytical field the use of preconcentrating materials is widely used to increase the concentration, or the amount, of trace components. Preconcentration also facilitates the sampling because allows the trace components to be isolated and determined, diminishing the sampling error and enhancing the sensitivity of an instrument[7]. The materials used for preconcentration of different analytes such as metals, explosives, drugs, VOCs, proteins are really various like fullerenes[8], organosilicas[9], metal-organic frameworks (MOFs)[10], cavitands[11], poly(methyl methacrylate) matrix covered with cellulose[12], nanoscale carbon-based materials[13] and generally other porous materials.

In our case, we deal with a very interesting challenge because we have the task to supply a material that is very fast both in sorption and in desorption of the targeted molecules. The only way to achieve this goal is to produce a material with high surface area and which allows rapid diffusion of molecules within it.

In the set up phase of the CUSTOM project, a micro- and nanoporous polymeric material has been selected. The first nanoporous polymer, syndiotactic polystyrene (sPS), has been described by Guerra and co-workers[14] ; moreover the same research group has recently discovered another nanoporous polymer, the poly(2,6-dimethyl-1,4-phenylene)oxide generally known as PPO[15]. Anyway, within the CUSTOM project, the selected preconcentrating material designed to concentrate targeted molecules is sPS. Its crystalline phase in the δ form, in fact, is nanoporous, that is it has very small pores with diameters of just few nanometers.

1.4 Nanoporous structures of syndiotactic polystyrene

The sPS shows a very complex polymorphic behaviour that can be described in terms of two crystalline forms, α and β, whose chains are in *trans*-planar zigzag conformation and two forms, γ and δ, containing helical chains in s(2/1)2

conformation[16]. More recently, another crystalline form of sPS, named ε, has been discovered[17]. The δ and ε forms are the only showing nanoporous crystalline phases: the former presenting isolated cavities (whose volume is around 120 Å^3)[14] in the crystalline structure, the latter has instead long channels, as shown in the representations of figures 1.5[18] and 1.6[19], respectively.

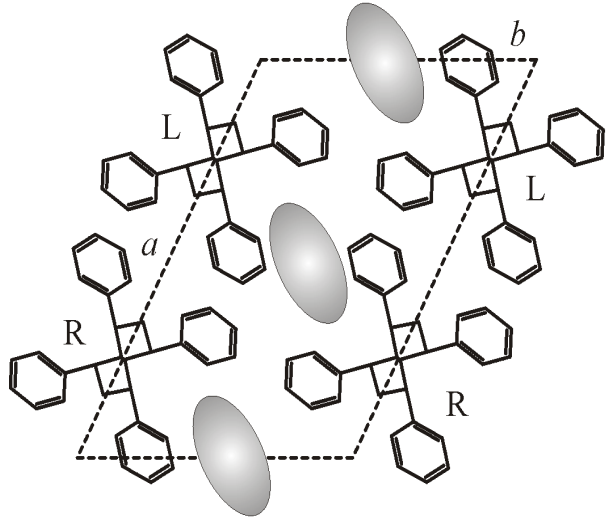

Figure 4.5 View of the host nanoporous crystalline δ form of sPS. Four adjacent unit cells along the c axis parallel to the (002) crystallographic plane. Each crystalline cavity (gray region) is confined by ten host phenyl rings.

The molecular chains in the δ form are packed in a monoclinic unit cell with axes a = 17.4 Å, b = 11.85 Å, c = 7.70 Å, and γ = 117° according to the space group $P2_1/a$[20]. This form is also characterized by two identical

cavities and eight styrene monomeric units per unit cell, with a crystalline density of 0.977 g/cm^3, lower than the density of the corresponding amorphous phase (1.055 g/cm^3)[20].

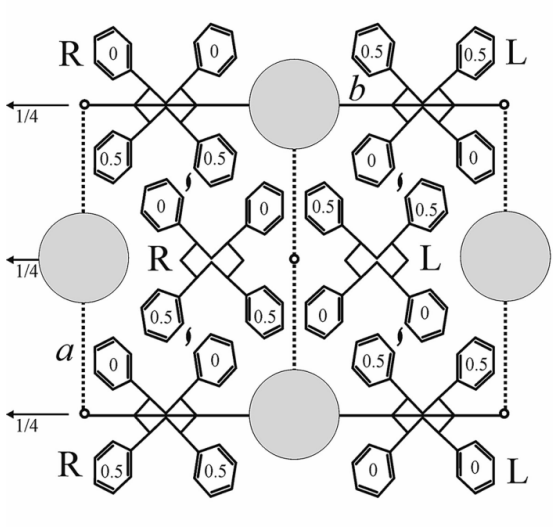

Figure 5.6 View along the c axis of the nanoporous ε form of sPS. Grey circles indicate the channels passing through all the crystal. R = right-handed, L = left-handed helical chains.

The unit cell proposed for the ε form, instead, is orthorhombic with axes a = 16.2 Å, b = 22.0 Å, c = 7.9 Å, and γ = 90°, belonging to the space group Pbcn[19]. Its crystalline density is 0.98 g/cm^3, similar to that one of the δ phase[21], with four chains of sPS in the s(2/1)2 helical conformation included in the unit cell.

Moreover, the δ and ε forms of sPS show the great ability to include in their crystalline structure, in cavities or in

channels respectively, low molecular mass guest molecules, forming co-crystalline molecular complexes called clathrates[22-23] and intercalates[23-24]. The sorption of such guest molecules from water and air occurs rapidly and selectively, also when these molecules are present at very low concentration.

Thus, the two nanoporous crystalline forms of sPS act as host to trap (and so to concentrate) guest molecules of suitable size, shape and polarity.

1.5 Microporous forms of syndiotactic polystyrene

In literature many microporous materials have been described, such as the most studied silica aerogels[25], and they are defined as materials containing pores with diameters less than 2 nm. Extremely porous materials with microporous cavities are described as aerogels. Also the δ form of sPS can be achieved in this morphology. The first sPS δ form microporous aerogels and their preparation have been described by Guerra and co-workers[26], and they are defined also nanoporous because they include a high percentage of crystalline δ phase of sPS, which is nanoporous. The sPS nanoporous δ form aerogel is obtained by removal, through CO_2 in supercritical conditions, of the solvent molecules from the micropores of the starting gel. We deal with a physical gel, in which the

polymer chains are connected by intermolecular physical bonding, that form junction zones. These junctions are the polymer-rich (or clathrate) phase of the gel and consist of crystalline regions[27]. The corresponding sPS nanoporous δ form aerogels derived from such physical gels present a fibrillar morphology, shown in figure 1.7.

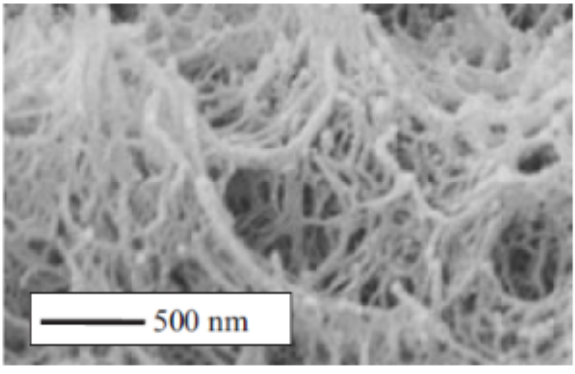

Figure 1.7 Scanning electron micrograph (SEM) of sPS δ form aerogel with fibrils of diameter between 50 and 100 nm.

In figure 1.8, instead, a schematic representation of the texture and of the crystalline structure of the sPS nanoporous δ form aerogel is reported[28].

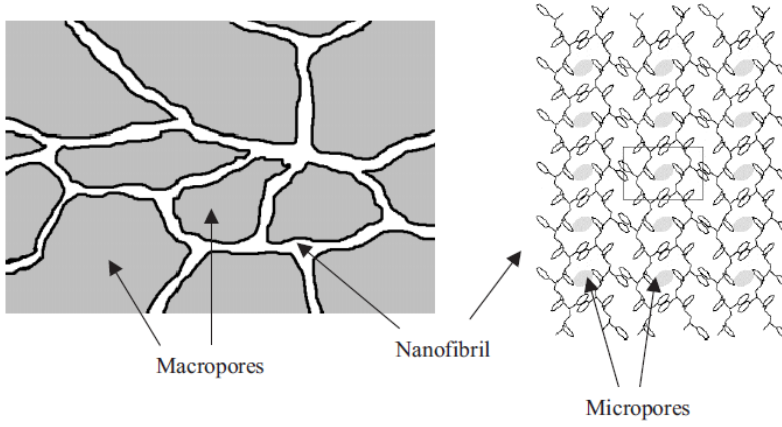

Figure 1.8 Schematic representation of the texture (left) and the crystalline structure (right) of the sPS δ form aerogels.

The sPS nanoporous δ form aerogels can be obtained in different porosity, depending on the concentration of the solvent used to prepare the starting gel[1]. Aerogels of sPS δ form with higher porosity show faster sorption and desorption kinetics; this behaviour is also due to the high surface area (about 290 m^2/g) typical for aerogels[26,28]. An example of the behaviour above mentioned is shown in the figure 1.9, where sorption and desorption kinetics of 1,2-dichloroethane (DCE) from 100 ppm aqueous solution at room temperature are shown for sPS nanoporous δ form aerogels with different porosity[1].

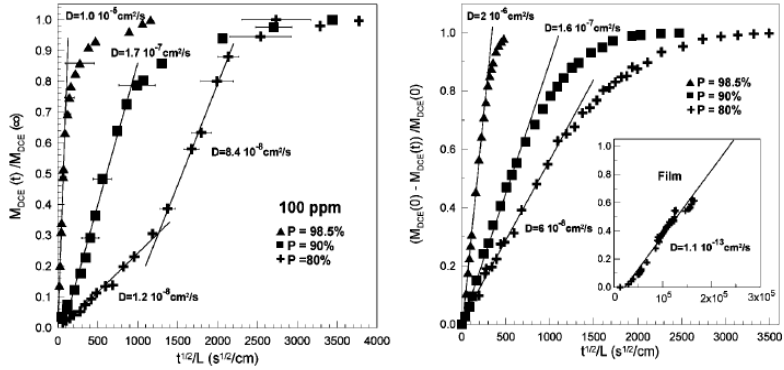

Figure 1.9 Sorption (left) and desorption (right) kinetics at room temperature of DCE from 100 ppm aqueous solutions for sPS nanoporous δ form aerogels with a porosity *P* = 98.5%(▲), *P* = 90%(■) and *P* = 80%(+).

Moreover, these materials also present a great sorption capacity, typical of sPS δ form and it is due to the sorption of molecules as isolated guests in its host nanoporous crystalline phase. This behaviour is widely reported in literature and here we show, just as an example in figure 1.10[28], the comparison in chloroform vapour sorption among a sPS nanoporous δ form aerogel, a β form sPS aerogel and a sPS nanoporous δ form film. Clearly is pointed out not only the much higher sorption capacity possessed by sPS nanoporous δ form aerogel respect to that of other forms of sPS aerogel, such as the β form, but also the much faster sorption kinetics of the aerogel respect to other morphologies such as the film.

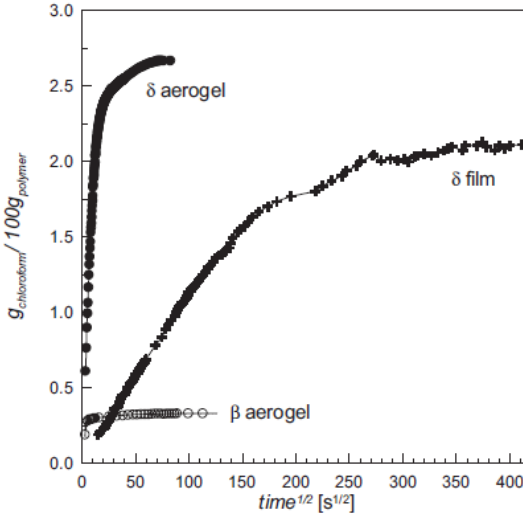

Figure 1.10 Chloroform vapor sorption kinetics obtained at $P_{chloroform}$ = 667 Pa and T = 56 °C for the δ (●) and β (○) form aerogels and for the δ form film (+).

Another example about the great sorption capacity of the δ form of sPS and the faster sorption kinetics of the aerogel respect to other morphologies, is illustrated in figure 1.11[1], where the comparison among aerogels of sPS δ form at different porosity, β form sPS aerogel, δ and γ form sPS powders are reported. Here, too, it is clear shown that the δ form of sPS is the one with the highest sorption capacity and that the aerogel morphology is the one showing the faster sorption kinetics.

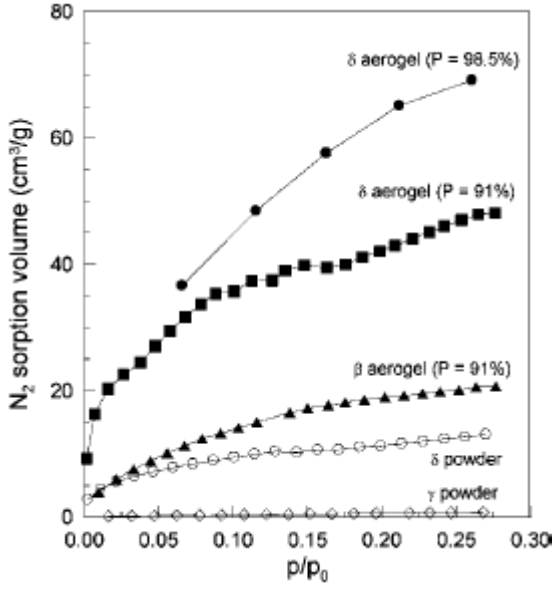

Figure 1.11. Nitrogen sorption isotherms in the range 0–0.30 p/p0 of δ-aerogels (P = 91% and 98.5%), β-aerogel (P = 91%), δ-powder, and γ-powder at 77 K. The sorption is expressed as cm^3 of nitrogen in normal conditions (1 atm, 273 K) per gram of polymer.

Aerogels of sPS δ form can be achieved in different shapes, such as monoliths, membranes, beads. This last shape has been found, by the ENEA agency CUSTOM partner who takes care of air sampling and developed PCU, the right one to fill in the slots of the PCU. The reasons of this choice are both the low hydraulic impedance, that is the minimization of pressure loss and optimization of air flow rate during air sampling, shown by the beads in some previous tests performed by ENEA, and the high surface area exposed to the air flow containing the precursors. We

obtained these beads of sPS nanoporous δ form aerogel in a range of 100-1000 μm, as shown in figure 1.12.

Figure 1.12 sPS nanoporous δ form aerogel beads in the size range 100-1000 μm.

Chapter 2
Results and discussion

2.1 Aerogel beads of sPS in nanoporous δ form: preparation and characterization

Studies carried out by ENEA unit of the CUSTOM consortium have shown that the bead morphology has low hydraulic impedance and good interaction surface, both desirable and suitable properties to make the PCU work in a correct and effective way. For this reason, the bead morphology has been chosen to test the behaviour of sPS towards the target drug precursors of the project.

It is well known that it is possible to obtain natural polymer aerogels in bead morphology [29-30], thus we developed a specific procedure to obtain sPS nanoporous δ form aerogels with this morphology

The preparation procedure, described in the experimental part (chapter 3, paragraph 3.2), requires that a polymer solution, with an appropriate concentration, is transferred still warm into a fluid dispenser which allows to have regular dropping at controlled rate. The polymer solution then drips through a syringe in an organic solvent held at low temperature (-80°C). The organic solvent has been properly selected among the non-solvents for the polymer,

so that the formed polymer solution drops coagulate in it forming gels with bead shapes.

The solvent is removed from the gel beads of sPS nanoporous δ form by extraction with CO_2 in supercritical conditions and sPS nanoporous δ form aerogel beads are achieved.

Aerogel bead samples were characterized by Fourier transform infrared spectroscopy (FTIR; figure 2.1) and wide angle X-ray diffraction (WAXD; figure 2.2). In figure 2.1, the whole FTIR spectrum is reported, even if the typical fingerprint of the sPS ranges between 1600 and 500 cm^{-1}. Just in this spectral region, the conformation and packing sensitive peaks of the nanoporous sPS δ form are present, located at 969, 944, 934, 548, 535, 503 cm^{-1}.[31] Moreover, the absence of chloroform bands (e.g the typically strong band at 1214 cm^{-1}) confirm that all the solvent of the gel has been surely removed from the polymer.

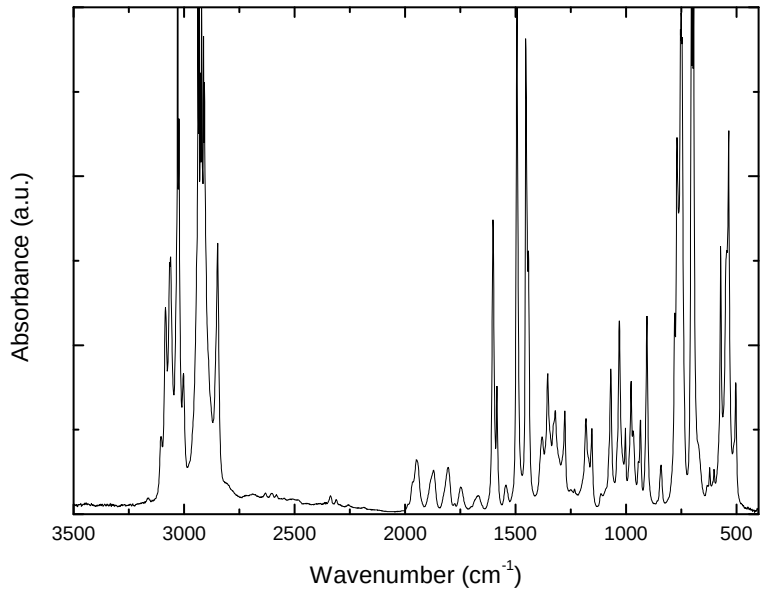

Figure 2.1. FTIR spectrum of sPS nanoporous δ form aerogel in bead morphology.

In the WAXD spectrum (figure 2.2) the typical pattern of the crystalline sPS nanoporous δ form[28], with the characteristic peaks at 2θ = 8.2, 13.6, 16.7, 20.7 and 23.5°, is present.

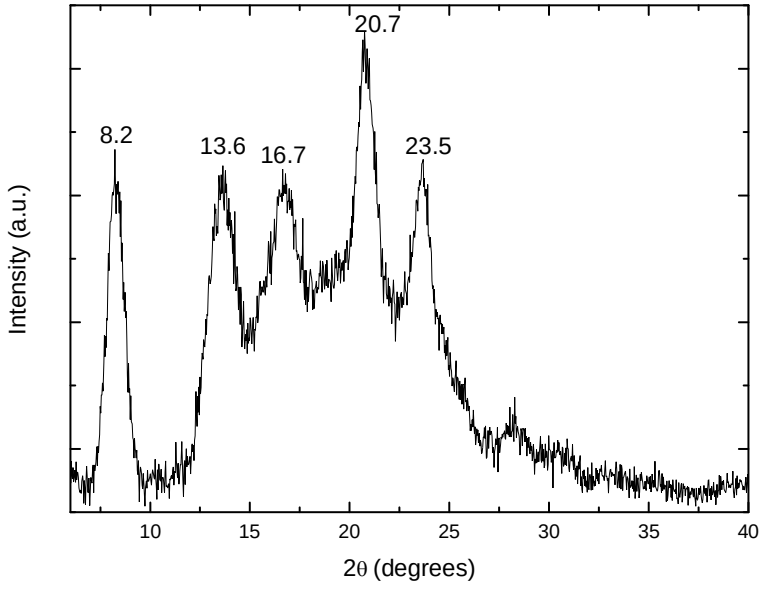

Figure 2.2. WAXD spectrum of sPS nanoporous δ form aerogel in bead morphology.

From X-ray diffraction and FTIR spectra, the degree of crystallinity of the sPS nanoporous δ form aerogel samples has also been evaluated and it resulted to be around 45% for all the samples obtained through the preparation procedure previously described.

The aerogel beads porosity has been also evaluated, for the different batches of beads produced, by using the procedure described by Daniel et al.[1] and reported in the experimental part (chapter 3, paragraph 3.4). Thus, a porosity in the range 87-91%, was evaluated for all the aerogel bead samples.

2.2 Drug precursors analyzed

As reported in chapter 1 paragraph 1.2, the CUSTOM project selected five drug precursors; among these ones we focused our attention on four of them, to test the CUSTOM prototype device: benzyl methyl ketone (BMK), ephedrine (Eph), safrole and acetic anhydride (AcAn), that are the most important, essential, the less replaceable and also the most trafficked and seized drug precursors used for illicit purposes.

Anyway, these precursors have also licit uses, for example BMK is used in the chemical industry for the synthesis of propylhexedrine (a vasoconstrictor used mainly to treat symptoms of nasal congestion due to colds, allergies and allergic rhinitis), and in the pharmaceutical industries for the production of methamphetamine and derivatives in medical applications. Eph is used as stimulant, appetite suppressant, concentration aid, decongestant, and to treat hypotension associated with anaesthesia. Safrole is used in perfumery, in the manufacture of piperonal (a molecule structurally related to benzaldehyde and vanillin, having a floral odour similar to that of vanillin and cherry), and to denature fats in soap manufacture. AcAn, instead, is used in chemical and pharmaceutical industries for manufacture of cellulose acetate, textile sizing agents and cold bleaching activators, polishing of metals, production of

brake fluids, dyes and explosives. The structures of the four precursors, whose transport properties within sPS nanoporous δ form aerogel were studied, are depicted in figure 2.3, together with the relative achievable psychotropic substances and the chemical reactions needed to obtain them.

For the CUSTOM project aims it is necessary to reveal such precursors when they are present in very low concentrations, but to identify the most relevant peaks in the FTIR and WAXD spectra as well as changes in thermogravimetric analysis (TGA) and mass spectrometer (MS) measurements, due to the behaviour and the influence of this precursors on the absorbing polymer, we started to perform tests at higher concentrations of this molecules.

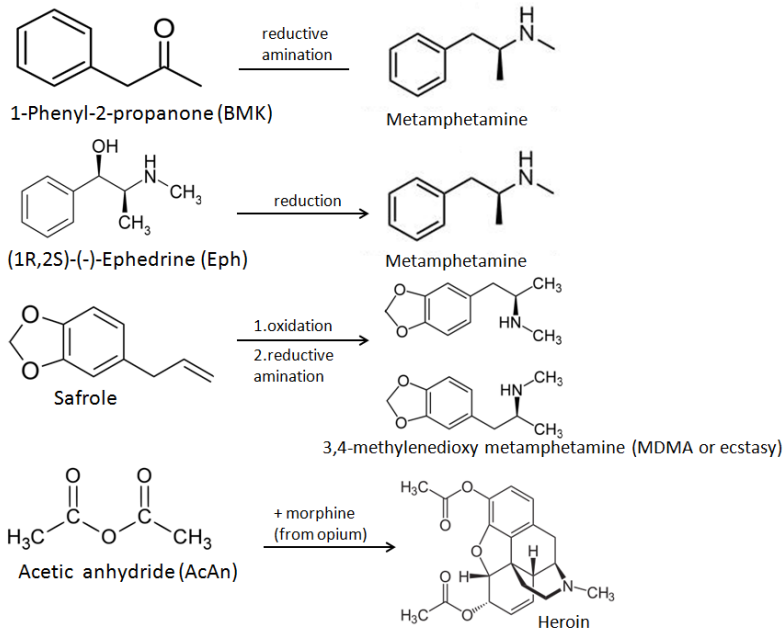

Figure 2.3 Drug precursors used to test the CUSTOM prototype device and relative psychotropic substances.

2.3 Benzyl methyl ketone (BMK)

In order to have a fast reply about the absorbing capacity of the polymer towards BMK and to easily identify the most intense FTIR and WAXD signals of BMK, a simple preliminary test was conducted exposing a sample of sPS nanoporous δ form aerogel to BMK vapours for 2 hours, at a temperature of about 40°C (temperature ensuring a relatively high BMK vapours pressure, which is 0.16 mm Hg at 25°C). The concentration in gas phase of BMK was evaluated to be around 840 ppm and the uptake of BMK in

the polymer, valued by TGA, was around 30% by weight, corresponding to a concentration factor (ratio between the concentration of the guest in the polymer and in the air) in the polymer of about 350. The nanoporous δ sPS aerogel sample after the BMK sorption was characterized by FTIR and WAXD and the results are reported in figures 2.4 and 2.5, respectively.

In figure 2.4 the FTIR spectrum of sPS aerogel sample after exposure to BMK vapours, and the same sample before the exposure, are compared. In the same figure, to make easier the comparison between the spectra, also the FTIR spectrum of the pure BMK is reported.

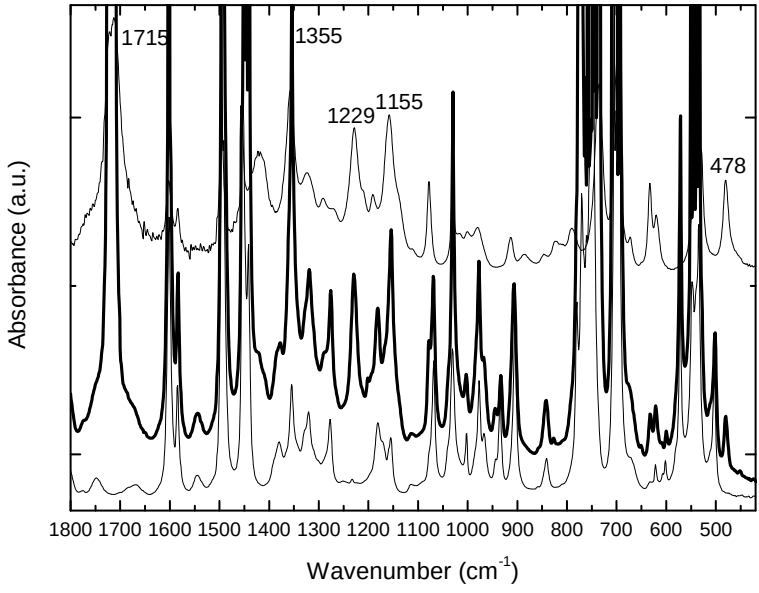

Figure 2.4 FTIR spectra of sPS nanoporous δ form aerogel (bottom), BMK absorbed in sPS nanoporous δ form aerogel (thick line) and pure BMK (top).

In the FTIR spectrum of the sPS nanoporous δ form aerogel sample exposed to BMK vapours, all the typical most intense infrared bands of BMK, e.g. those at 1715, 1355, 1229, 1155 and 478 cm^{-1} labelled in figure, are present. The the infrared bands at 1715 and 1355 cm^{-1} are in saturation condition, i.e. the intensity of these bands fall out from the range of linear response given by the law of Lambert-Beer. It is worth noting that the infrared absorbance region showed in figure corresponds to the wavenumbers range in which the main absorbance bands of the polymer and BMK are present.

In the figure 2.5, the WAXD spectra of a sPS nanoporous δ form aerogel sample exposed to BMK vapours (top) and of the same sample before the exposure (bottom), are reported.

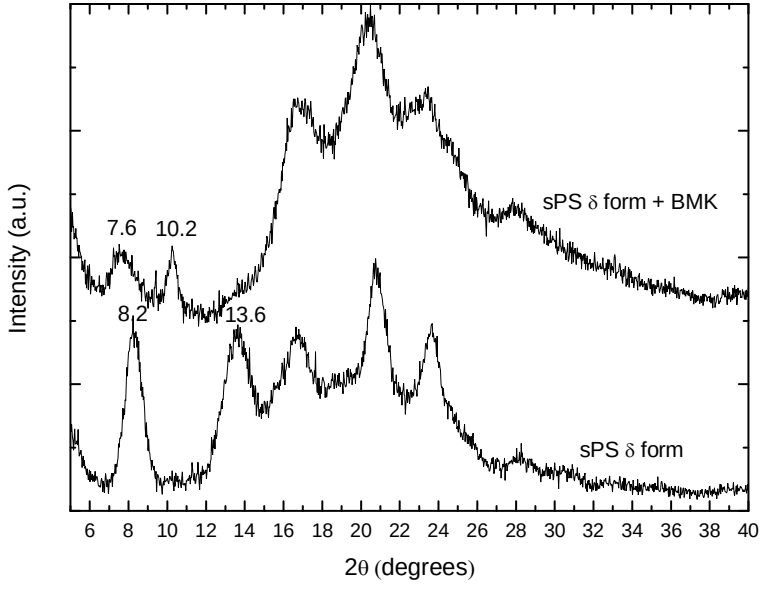

Figure 2.5 WAXD spectra of sPS nanoporous δ form aerogel (bottom) and of sPS nanoporous δ form aerogel exposed to BMK vapours (top).

They are worth noting the differences in some reflections between the two diffraction spectra of fig.2.5. The enhancement of the reflection intensity at 2θ = 10.2° and the depression of those at 2θ = 8.2 (also shifted to 7.6°) and 13.6°, observed in the sample exposed to BMK vapours (top curve in figure), mean that some changes in the polymer crystalline structure, due to the sorption of

BMK, occurred. This WAXD pattern is characteristic of a sPS co-crystalline structure [20], in which guest molecules are included in the crystalline cavities of the nanoporous δ sPS (host). The shift of the reflection from 2θ = 8.2° to values < 8°is typical of a sPS clathrate structure. The presence of a guest molecule enlarges the unit cell (mostly the b axis) so that, also molecules that are definitely larger than the cavity of the sPS δ form, make stable clathrates[14]. In this case, the estimated amount of the cavities of the crystal lattice of sPS δ form filled by BMK molecules resulted to be around 90%.

In order to verify the effectiveness of BMK sorption in sPS nanoporous δ form aerogel samples also when BMK is present in low concentrations (the typical working conditions supposed for the CUSTOM designed device), a series of sorption experiments from aqueous solution at different BMK concentration (1, 10, 50, 100, 250 and 500 ppm) have been performed. A more detailed description of these experiments is reported in the experimental part (chapter 3, paragraph 3.5).

FTIR and WAXD measurements of sPS nanoporous δ form aerogel samples exposed to BMK aqueous solutions are shown in the figures 2.6 and 2.7, respectively.

In figure 2.6, the FTIR spectra in the regions 1100-1300 cm^{-1} and 1600-1800 cm^{-1} of all the sPS nanoporous δ form

aerogel samples exposed to BMK aqueous solutions, are reported. It is worth nothing that the considered spectral regions are those in which the most intense infrared bands of BMK (1715, 1229 cm^{-1}), not overlapping to sPS absorbance bands, are present.

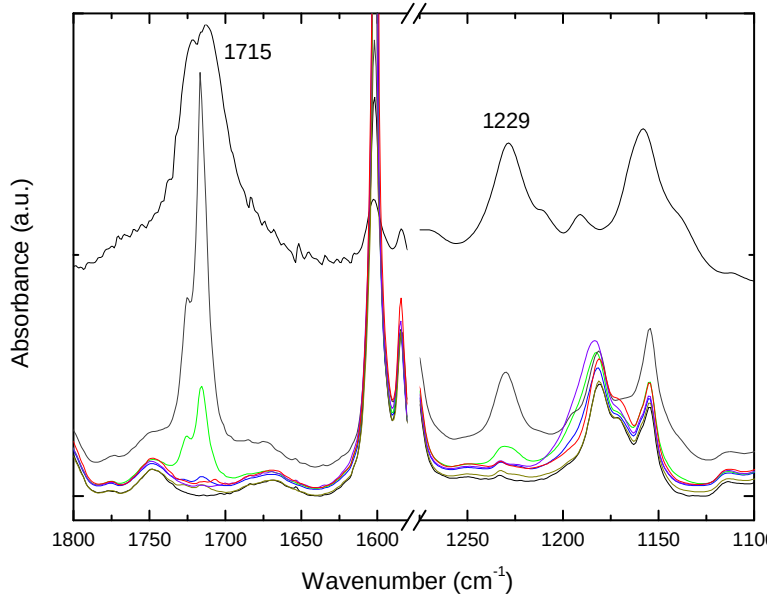

Figure 2.6 FTIR spectra of sPS nanoporous δ form (bottom), pure BMK (top) and sPS nanoporous δ form samples exposed to BMK 1, 10, 50, 100, 250 and 500 ppm aqueous solutions.

The percent of guest uptake in each sPS aerogel sample immersed in a BMK aqueous solution is reported in Table 2.1. These percentages have been evaluated through two calibration lines, one for the highest concentrations and the other for the lower ones, built as described in chapter

3, paragraph 3.6, that correlates the intensity of the BMK absorbance bands in FTIR with the results of TGA measurements.

Table 2.1. BMK uptake in nanoporous δ sPS aerogel samples immersed in BMK aqueous solutions.

BMK aqueous solution	BMK uptake
1 ppm	0.9 %
10 ppm	0.8 %
50 ppm	0.9 %
100 ppm	1 %
250 ppm	5 %
500 ppm	10 %

In figure 2.7, the WAXD spectra of the sPS nanoporous δ form aerogel samples immersed in BMK aqueous solutions at different concentrations, are shown.

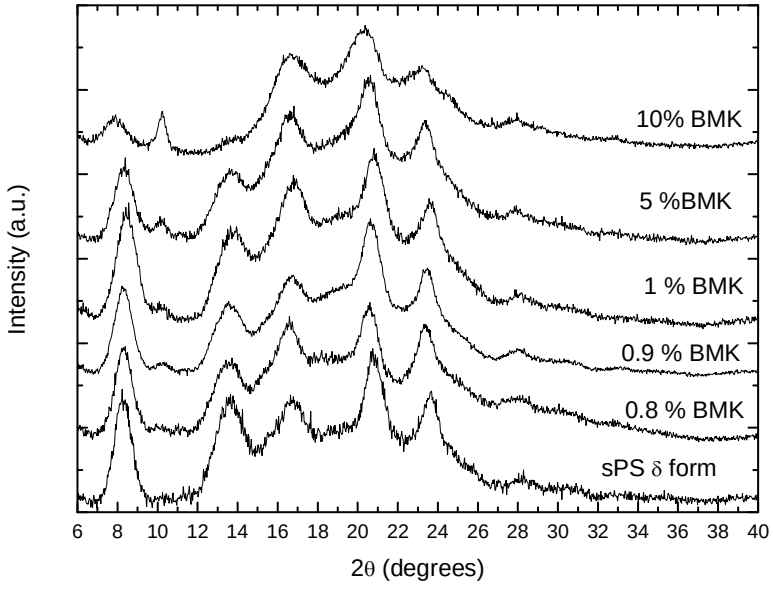

Figure 2.7 WAXD spectra of sPS nanoporous δ form aerogel (bottom) and of sPS nanoporous δ form aerogel samples immersed in BMK aqueous solutions at different concentrations. The BMK uptake is also reported.

It is clear that as the BMK content in the samples increases, the intensity of the reflection at 2θ = 10.2° is enhanced as well as the intensity of the reflections at 2θ = 8.2° and at 2θ = 13.6° is reduced. In particular, when the BMK uptake is 10% (test performed in 500 ppm aqueous solution) the WAXD pattern is characteristic of a sPS co-crystalline structure [20], in which guest molecules are included in the crystalline cavities of the sPS nanoporous δ phase. For this sample, the calculated amount of the

cavities of the crystal lattice of sPS nanoporous δ form filled by BMK molecules resulted to be about 35%.

The BMK equilibrium uptake values vs the BMK aqueous solution concentrations are reported in figure 2.8. The BMK equilibrium uptake values has been valued by FTIR measurements, as reported in experimental section chapter 3 paragraph 3.6, considering the BMK absorbance bands at 1715 and 1229 cm^{-1}.

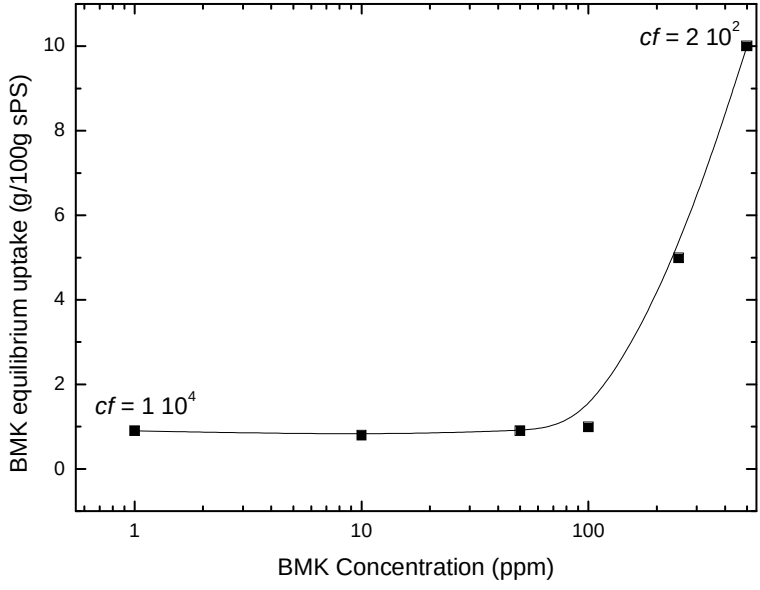

Figure 2.8 BMK equilibrium uptake vs BMK concentration in aqueous solution; *cf* of 1 and 500 ppm BMK aqueous solutions are also shown.

For two points, corresponding to 1 and 500 ppm BMK concentration, of the sorption curve in figure 2.8 the concentration factor (*cf*), that is the ratio between the

concentration of the guest in the polymer and in aqueous solution, is also reported.

It is worth noting that the *cf* in the polymer increases as the BMK concentration in the aqueous solution decreases, passing from $2 \cdot 10^2$ when the concentration of BMK solution is 500 ppm, up to $1 \cdot 10^4$ when the concentration of BMK solution is 1 ppm[32].

These data indicate that the sPS in nanoporous δ form is highly effective in concentrating the drug precursor molecules when presents at very low concentration in the environment.

These data are in well agreement with the polymer behaviour described by Daniel et al. [1,33] with other molecules, such as 1,2-dichloroethane (DCE). An example of this similar behaviour is shown in figure 2.9, where DCE equilibrium uptake is reported versus DCE concentration in aqueous solution [1].

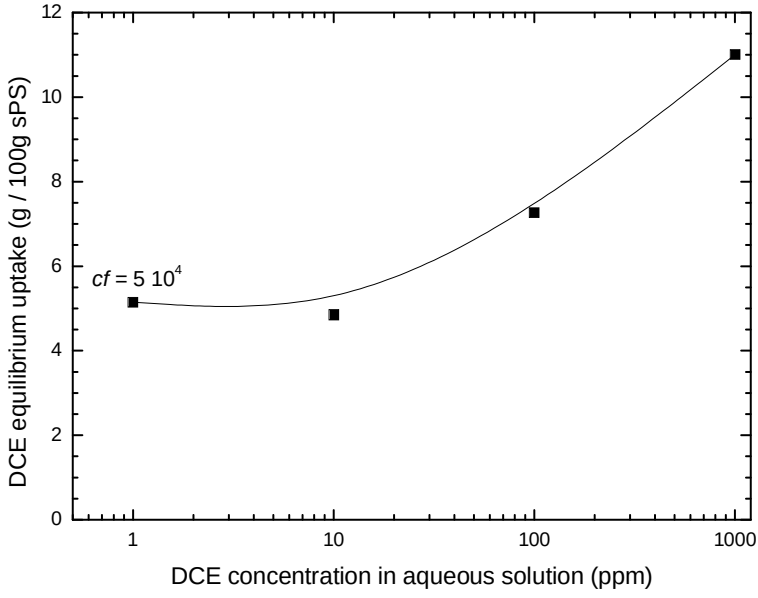

Figure 2.9 DCE equilibrium uptake vs. DCE concentration in aqueous solution; *cf* of 1 ppm DCE aqueous solution is also shown. Data from ref. 1.

As you can see, the trend of the values of the equilibrium uptake curve and the effectiveness in DCE sorption are very similar to those ones shown for the BMK (compare the cf reported in figure 2.9 with that one reported in figure 2.8), showing that this behaviour is characteristic of the semicrystalline δ form of sPS. Apparently, the nanocavities in the crystalline phase of δ sPS are capable to trap and concentrate the guest molecules in a very effective way when they are in very low concentrations.

2.4 Ephedrine

In order to verify the sorption capacity of the sPS nanoporous δ form aerogel towards ephedrine (Eph), preliminary tests were conducted by exposing a polymer sample to Eph vapours for about 2 hours at 40°C (increasing Eph vapour pressure, that is 0.009 mmHg at 25°C). The FTIR spectroscopy measurements on this polymer sample have shown that sPS nanoporous δ form aerogel is not able to absorb this precursor. Further Eph sorption tests were conducted immersing polymer aerogel samples in Eph aqueous solutions at different concentrations, but the sorption of this precursor did not occur neither in these cases.

We tried to dissolve Eph in solvents, like acetone, chloroform, ethanol, acting as a carrier for this precursor into the polymer, but it was not absorbed.

We initially attributed these behaviours to a lack of affinity between Eph and the sPS nanoporous δ form aerogel, being the former a polar molecule and the second a non-polar polymer. Then, it is very likely that Eph is not soluble in the polymer.

We thought to make partially polar the polymer by selectively functionalizing only its amorphous phase with sulfonic groups[34], which could potentially be able to absorb Eph. Unfortunately, not even in this case the sulfonated

sPS nanoporous δ form aerogel was able to absorb Eph, neither from its vapours nor from aqueous solutions at different concentrations.

Probably, Eph tends to be associated perhaps in the form of dimer, so its dimensions are too big for the cavities of the nanoporous sPS δ form. However, also in the nanoporous sPS ε form this precursor is not absorbed.

2.5 Safrole

As previously shown for the BMK, to quickly know which is the sorption capacity of the polymer towards safrole and what are the characteristic signals of safrole for an easy identification, we performed a preliminary test by simply exposing a sPS nanoporous δ form aerogel sample to safrole vapours for 30 minutes, at a temperature of about 40°C (to increase safrole vapour pressure, that is 0.07 mmHg at 25 C). The safrole concentration in the vapour phase was around 470 ppm and the uptake of safrole in the polymer was 20%, as arose from TGA measurements. Moreover, the valued amount of the cavities of the crystal lattice of sPS nanoporous δ form filled by safrole molecules in this sample is around 50%.

The sPS nanoporous δ form aerogel sample after the safrole sorption was characterized by FTIR and WAXD measurements, whose spectra are reported in figure 2.10

and 2.11, respectively.

In figure 2.10, the FTIR spectra of the polymer sample after exposure to safrole vapours and before the exposure are compared. Moreover, for an easier comparison between the spectra, the FTIR spectrum of the pure safrole is shown.

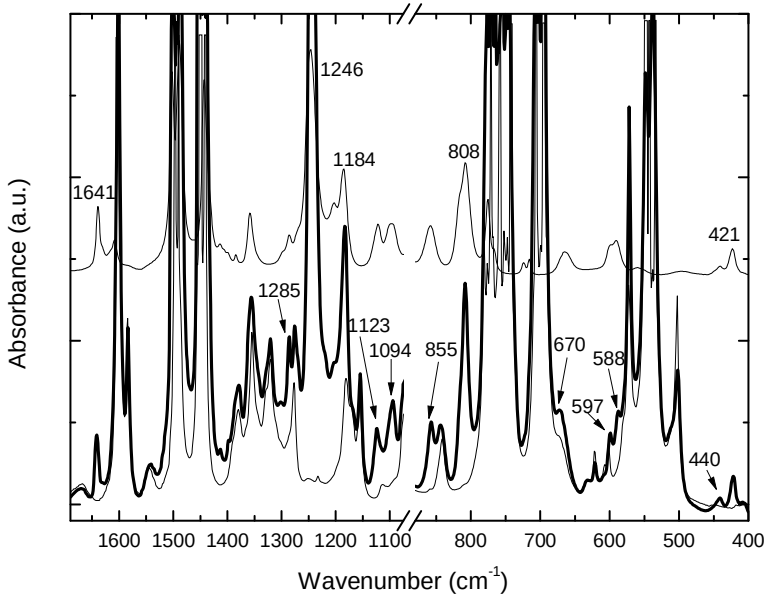

Figure 2.10 FTIR spectra of sPS nanoporous δ form aerogel (bottom), safrole absorbed in sPS nanoporous δ form aerogel (thick line) and pure safrole (top).

In the FTIR spectrum of the polymer sample exposed to safrole vapours, the characteristic most intense infrared bands of safrole at 1641, 1285, 1246, 1184, 1123, 1094, 855, 808, 670, 597, 588, 440 and 421 cm^{-1} labelled in

figure, are present. The infrared band at 1246 cm^{-1} is in saturation condition, i.e. it does not fall in the range of linear response of the Lambert-Beer law, while some bands are labelled with arrows for clarity. The infrared absorbance region reported in figure is that in which the main absorbance bands of sPS and safrole are evident.

In figure 2.11, the WAXD spectra of the nanoporous δ sPS aerogel sample exposed to safrole vapours (top) and of the same sample before exposure (bottom) are reported.

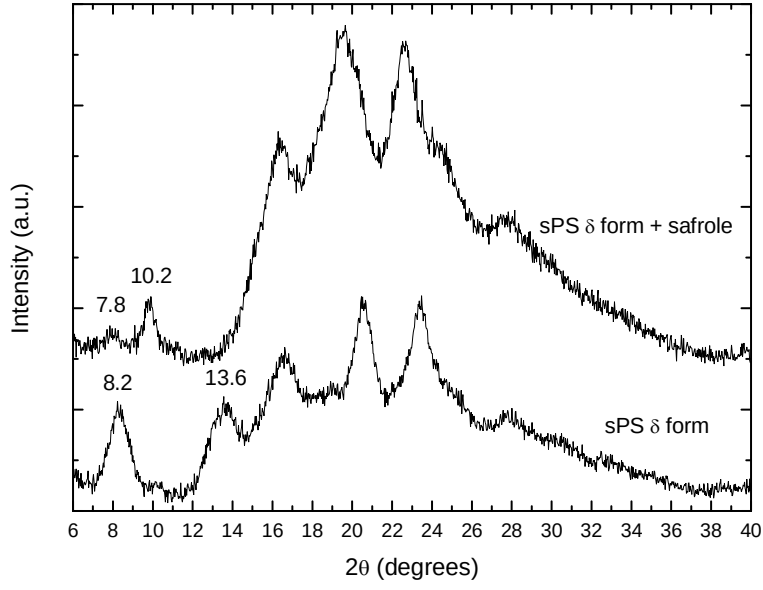

Figure 2.11 WAXD spectra of sPS nanoporous δ form aerogel (bottom) and of sPS nanoporous δ form aerogel exposed to safrole vapours (top).

The WAXD pattern of the sample exposed to safrole

vapours (top curve in figure 2.11) is typical of a sPS co-crystalline structure[20], in which safrole forms a host/guest complex with the sPS nanoporous δ form. Comparing the WAXD spectrum of the polymer exposed to safrole vapours (top curve figure 2.11) with that one of polymer exposed to BMK vapours (top curve figure 2.5), you can see that the intensity of the peak at $2\theta = 7.8°$ is much lower in the former case than in the latter. This datum can be explained considering the bigger size and weight of safrole with respect to BMK.

Likewise to what done for the BMK, we performed some experiments from aqueous solutions at different safrole concentrations (1, 10, 25 and 50 ppm). A detailed procedure of the performed tests is reported in the experimental part (chapter 3, paragraph 3.5).

The FTIR and WAXD measurements of all sPS nanoporous δ form aerogel samples immersed in safrole aqueous solutions are shown in figures 2.12 and 2.13, respectively.

In figure 2.12, only the ranges between 1670-1580 cm^{-1} and 880-400 cm^{-1} are shown, because the most intense infrared absorbance bands of safrole at 1641, 855, 808, 670, 597, 588, 440 and 421 cm^{-1} labelled in figure, which do not overlap with those ones of sPS, are present. It is noteworthy that the infrared bands at 1641, 808 and 588 cm^{-1} do not follow the linearity of the law of Lambert-Beer,

so they are in saturation condition, and that some bands are marked with arrows for clarity.

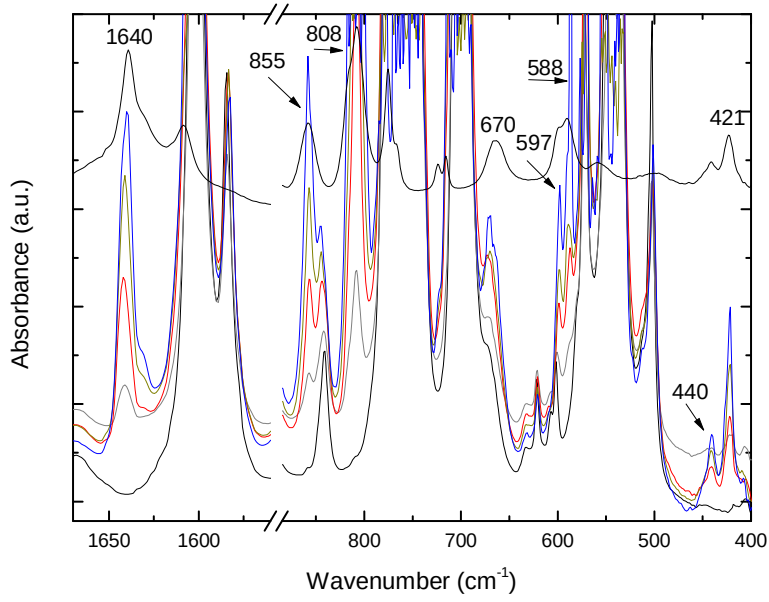

Figure 2.12 FTIR spectra of sPS nanoporous δ form aerogel(bottom), pure safrole (top) and sPS nanoporous δ form samples exposed to safrole 1, 10, 25 and 50 ppm aqueous solutions.

In Table 2.2, the amount of safrole uptake in the sPS aerogel samples immersed in the safrole aqueous solutions is reported. These values have been calculated through a calibration line, described in chapter 3, paragraph 3.6, in which the intensity of the safrole absorbance bands in FTIR and TGA data are correlated.

Table 2.2. Safrole uptake in sPS nanoporous δ form aerogel samples immersed in safrole aqueous solutions.

Safrole aqueous solution	Safrole uptake
1 ppm	5 %
10 ppm	15 %
25 ppm	24 %
50 ppm	33 %

The WAXD spectra of the sPS nanoporous δ form aerogel samples immersed in safrole aqueous solutions at various concentrations are reported in figure 2.13. It is evident the enhancement of the intensity of the reflections at 2θ = 10.2°, while the intensity of the reflections at 2θ = 8.2 (shifted to 7.8°) and 13.6° is reduced, as the safrole amount in the sPS samples increases. All the X-ray diffraction patterns shown are typical of a co-crystalline structure between the host polymer and the guest molecule[20]. For the sample whose safrole uptake is 33% (corresponding to the test performed with 50 ppm aqueous solution), the cavities of the crystal lattice of sPS nanoporous δ form filled by guest molecules resulted to be around 80%.

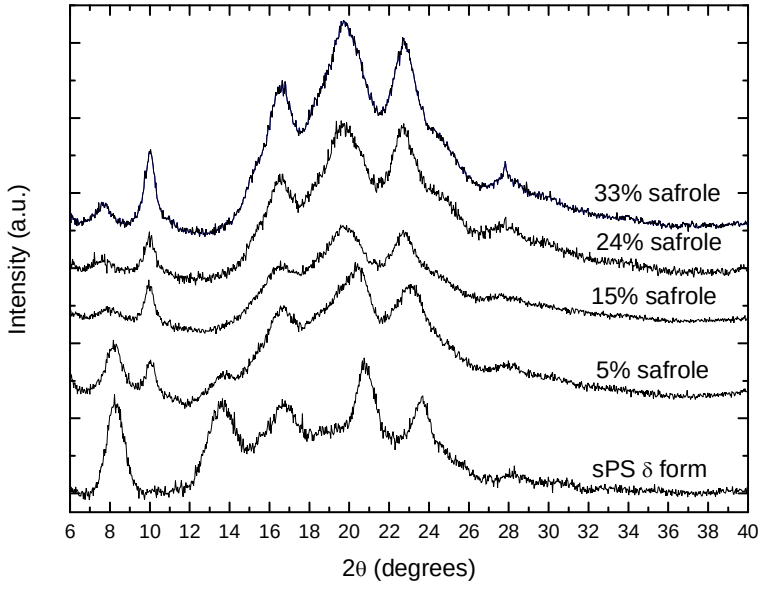

Figure 2.13 WAXD spectra of sPS nanoporous δ form aerogel (bottom) and of sPS nanoporous δ form aerogel samples immersed in safrole aqueous solutions at different concentrations. The safrole uptake is also reported for each spectrum.

The safrole equilibrium uptake values vs safrole aqueous solutions concentrations are reported in figure 2.14. The data of the figure have been evaluated by FTIR measurements, as reported in the experimental part (chapter 3, paragraph 3.6), on the basis of the safrole infrared absorbance band at 1640 cm^{-1}.

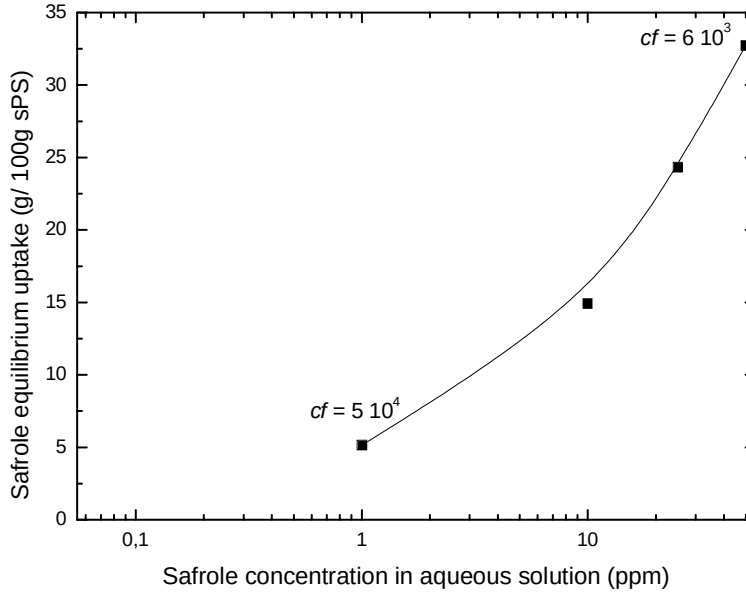

Figure 2.14 Safrole equilibrium uptake vs. safrole concentration in aqueous solution; *cf* of 1 and 50 ppm safrole aqueous solutions are also shown.

For the lowest and the highest value on the sorption curve of figure 2.14, corresponding to 1 and 50 ppm safrole aqueous solution concentration, respectively, the *cf* is reported. It is remarkable the enhancement of *cf* moving from a higher concentration to a lower one. In fact, the *cf* passes from $6 \cdot 10^3$ at safrole concentration in solution of 50 ppm, to $5 \cdot 10^4$ when safrole concentration in solution is 1 ppm[32]. These data show that the sPS nanoporous δ form aerogel is highly effective to concentrate safrole too, even if it is present in low concentrations.

Also in the case of safrole, as already seen for BMK; the data and the trend of the sorption equilibrium uptake curve are in good agreement with the behaviour of sPS described by Daniel and co-workers[1,33].

2.6 Acetic Anhydride (AcAn)

The last precursor tested for the aims of the CUSTOM project is the acetic anhydride (AcAn). As in the previous cases, a sample of sPS nanoporous δ form aerogel has been exposed to AcAn vapours, for 2 minutes at about 25°C since AcAn is quite volatile (its vapour pressure at 20°C is 4 mmHg and the concentration of AcAn in air was about 16000 ppm), in order to verify the sorption capacity of sPS towards AcAn and to identify the main signals of this precursor. By TGA we were able to evaluate the uptake of AcAn within the polymer, that is around 4%, corresponding to the 17% of filled cavities in the crystal lattice of sPS nanoporous δ form by AcAn molecules. On the nanoporous δ sPS sample exposed to AcAn vapours, FTIR and WAXD measurements have been performed, as shown in figure 2.15 and 2.16 respectively.

In figure 2.15, the FTIR spectra of the polymer after AcAn exposure and before this exposure are reported for comparison. Moreover, the FTIR spectrum of pure AcAn is shown for clarity. In the infrared absorbance spectrum of

the sPS aerogel sample exposed to AcAn vapours, all the typical most intense absorbance bands of AcAn, i.e. those at 1829, 1756, 1367, 1226, 1128 and 996 cm^{-1} also labelled in figure, are present.

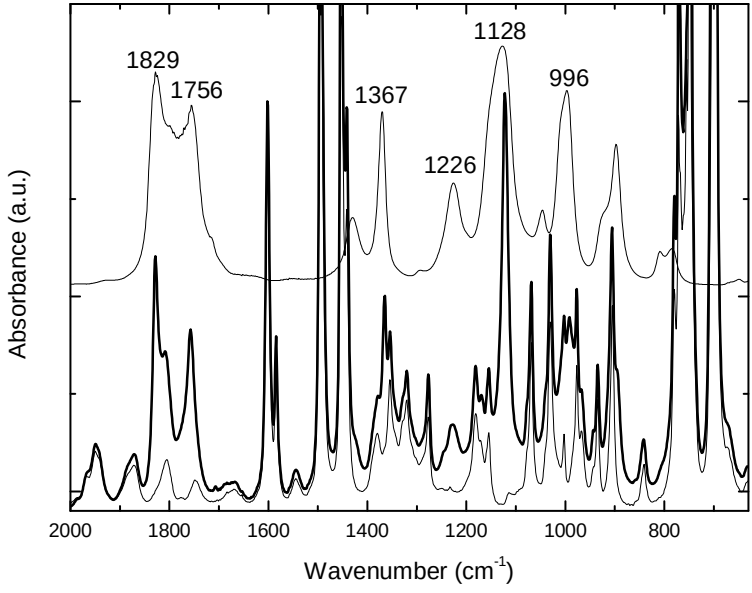

Figure 2.15 FTIR spectra of sPS nanoporous δ form aerogel (thin line, bottom), AcAn absorbed in sPS nanoporous δ form aerogel (thick line) and pure AcAn (thin line, top).

Moreover, the WAXD spectra of figure 2.16 confirm that the sorption of AcAn also occurs in the crystalline phase of the polymer, as illustrated by the typical co-crystalline structure pattern of the sPS nanoporous δ form aerogel exposed to AcAn vapours (top)[20].

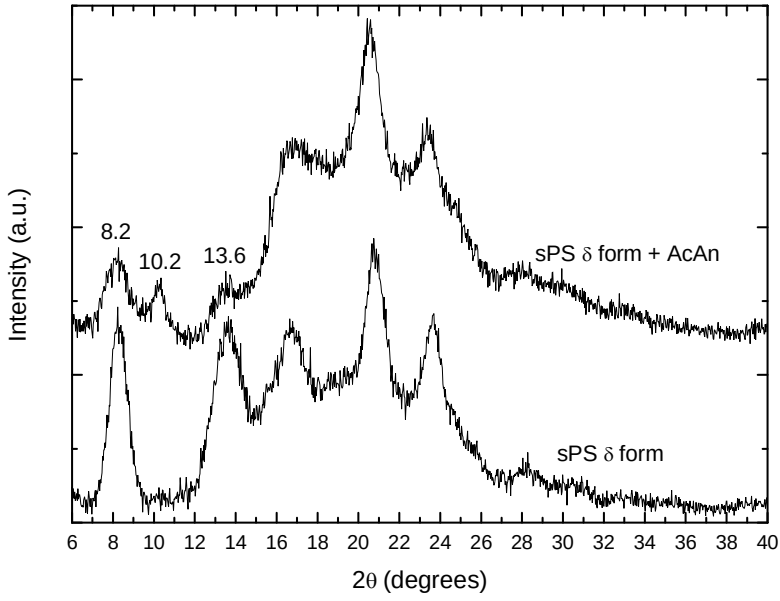

Figure 2.16 WAXD spectra of sPS nanoporous δ form aerogel (bottom) and of sPS nanoporous δ form aerogel exposed to AcAn vapours (top).

Unlike the previous precursors studied, BMK and safrole, AcAn hydrolyzes in water forming acetic acid. For this reason, it was not possible to prepare aqueous solutions of AcAn to control its concentration. Anyway, to test the effectiveness of sPS nanoporous δ form aerogel in concentrating AcAn at low concentrations, we performed some experiments in gas phase with a proper homemade apparatus[35], which is able to produce an air flow containing one or more analytes in low concentrations.

The apparatus used is shown in figure 2.17 and it included also the PCU, whose tasks were to accommodate the

beads of polymer in its slots and to control temperature, thanks to Peltier elements, and air flow.

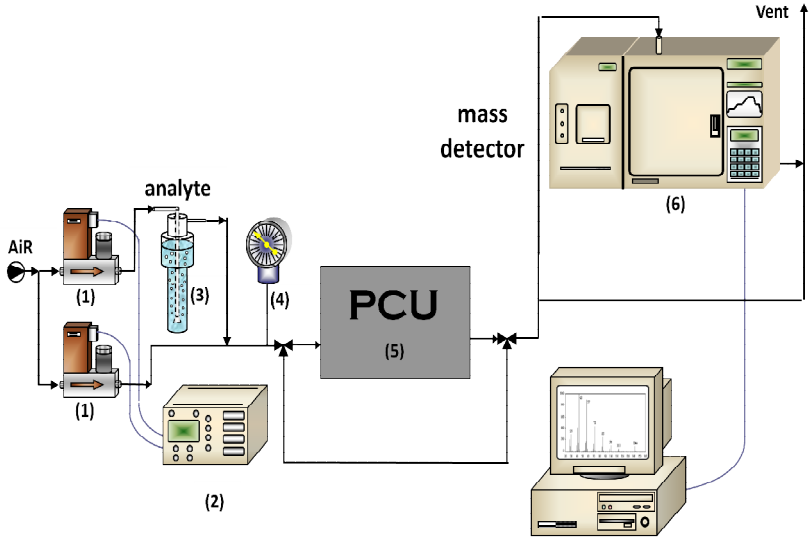

Figure 2.17. Apparatus to produce air flow containing analytes: (1) mass flow controllers; (2) mass flow controllers control unit; (3) analyte saturator; (4) manometer; (5) preconcentrator; (6) mass spectrometer.

In the apparatus shown above, the air flow containing a well defined amount of AcAn, which is regulated by mass flow controllers (MFC) and MFC control unit, passes through the PCU and then is send to the mass spectrometer (MS) detector. A simplified scheme of the profiles of sorption and desorption processes is shown in figure 2.18.

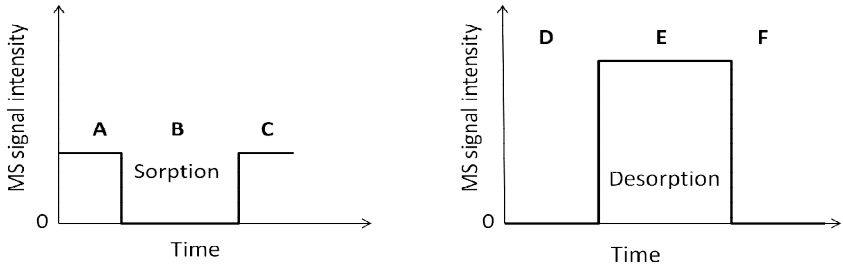

Figure 2.18. Scheme of the sorption (left) and desorption (right) processes.

On the left of figure 2.18, the profile of sorption process at a certain concentration of AcAn is depicted. At the beginning of the measurement, the air flow containing a mixture of air and AcAn does not pass through the PCU and it is detected by MS, which gives a constant signal intensity (**A**). As soon as the air flow passes through PCU, the sorption process occurs (**B**) and continues until the signal intensity reaches the starting level again (**C**). During the sorption, that is an exothermic process, the Peltier elements of the PCU are held at low temperature.

After the complete sorption of AcAn by the polymer, the temperature is increased up to 50°C to allow the desorption (that is an endothermic process) of the precursor. For the desorption process the intensity of the MS signal is dropped to zero (**D**). When desorption occurs (**E**),the intensity of the MS signal increases of several times with respect to the starting level. When all the AcAn has

been desorbed, the intensity of the MS signal returns to zero (**F**).

Hence, with the system above described, we were able not only to test the effectiveness of the polymer in the AcAn sorption at low concentrations, but also to validate the PCU working conditions.

The mass flow of AcAn to be set to the MFC control unit, considering a mixture made of air and AcAn, is calculated starting from Raoult's law, as reported in the experimental part (chapter 3, paragraph 3.7).

The working conditions used to perform the tests on sorption/desorption of AcAn were the following:

- temperature of PCU during sorption: 15°C
- temperature of PCU during desorption: 50°C
- air flow used in the sorption tests: 128 NL/h
- air flow used in the desorption tests: 60 NL/h

The AcAn concentrations tested for the sorption and desorption of this guest in beads of sPS nanoporous δ form aerogel were 5, 10, 20, 40 and 100 ppm[36].

In figure 2.19 is reported an example of the MS detector response in a sorption/desorption cycle of AcAn in the beads of nanoporous δ sPS aerogel. In this figure, the initial concentration of AcAn is 5 ppm. It is worth noting that the intensity of the signal given by MS detector is

proportional to AcAn concentration, according to the calibration line described in the experimental part (chapter 3, paragraph 3.6).

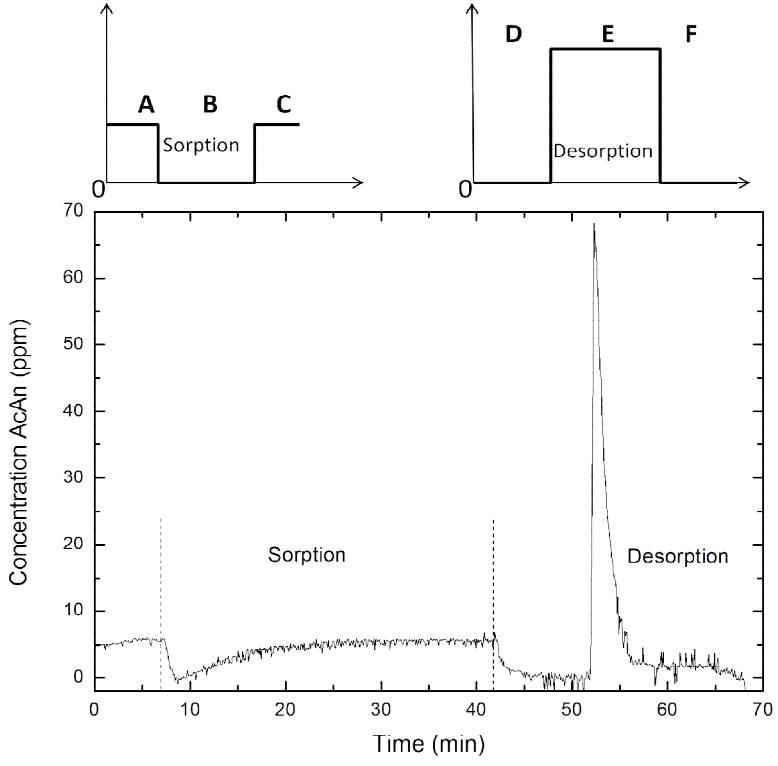

Figure 2.19. Example of the sorption/desorption cycle of AcAn in beads of sPS nanoporous δ form aerogel. AcAn concentration in air flow: 5 ppm.

On the top of the figure, for major clarity, the sorption and desorption schemes are also reported. The sorption begins at t=7.2 min and lasts until t=41.5 min. After that the temperature of PCU is increased from 15 to 50°C and the desorption begins (t=51.3 min), giving rise to the high peak

containing 67 ppm of AcAn, so the precursor has been concentrated of about 13 times with respect to its initial 5 ppm concentration.

As already done for BMK and safrole, the curve of absorbed AcAn equilibrium uptake at different concentrations is reported in figure 2.20. The values of the curve were obtained by integration of AcAn concentration profiles during the sorption phase.

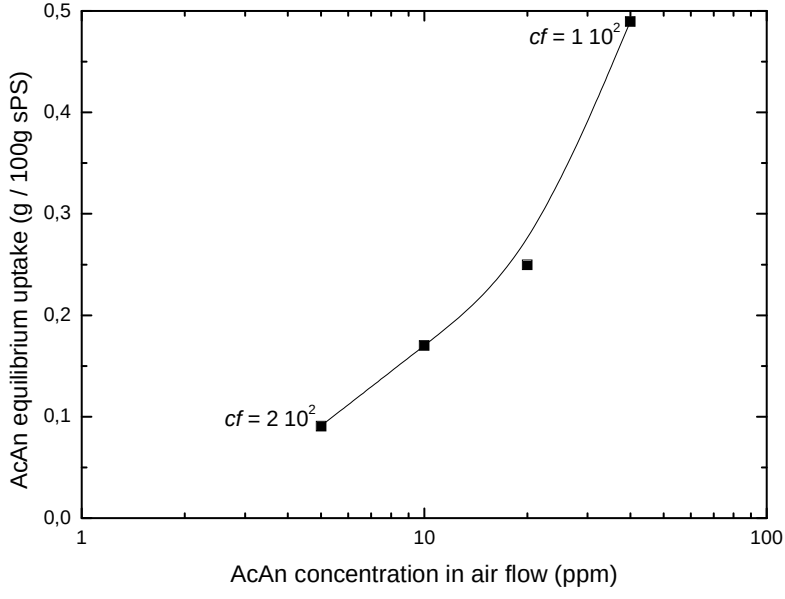

Figure 2.20 AcAn equilibrium uptake vs. AcAn concentration in air flow; *cf* of AcAn in air flow at 5 and 40 ppm are also shown.

On the sorption curve of figure 2.20 there are also shown the *cf* for the AcAn concentrations in air flow at 5 and 40 ppm, that are $2 \cdot 10^2$ and $1 \cdot 10^2$ respectively[32]. Once again,

at the lowest initial concentration of the precursor corresponds the highest *cf* within the polymer.

The experimental apparatus allowed us to gain also information about the kinetics of AcAn sorption and desorption, as shown in the following figures. In figure 2.21 the amount of AcAn absorbed by the polymer in the PCU vs sorption time is reported, and for each curve the AcAn concentration in the inlet air has been indicated. It is already clear from this figure that, in about 16 minutes, the beads of sPS nanoporous δ form aerogel are saturated by AcAn flow, whatever the AcAn concentration in the inlet air is.

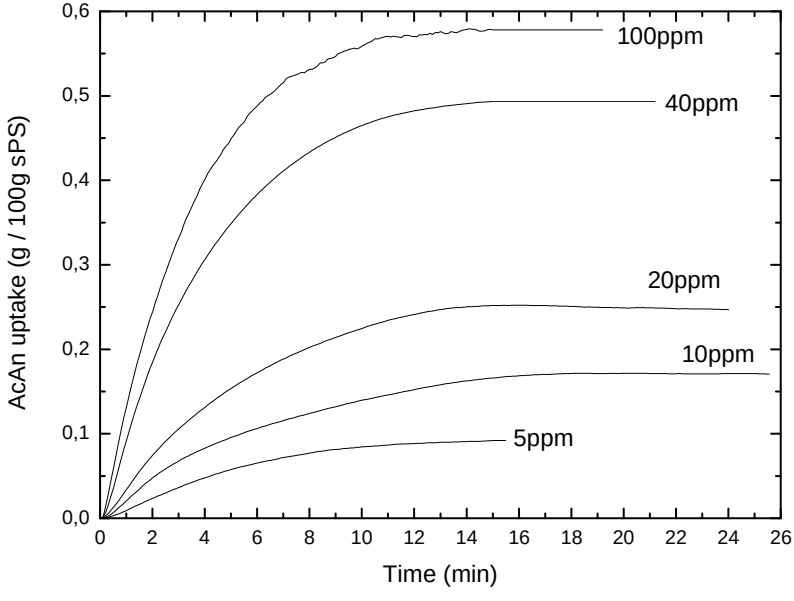

Figure 2.21 Amount of AcAn absorbed by the polymer vs the sorption time. For each curve the initial AcAn concentration has indicated.

In figures 2.22 and 2.23 the sorption and desorption kinetic curves are respectively depicted. These kinetic curves are in normalized form, i.e. M_t/M_∞ vs time$^{1/2}$. The subscripts t and ∞ refer to mass (M) of AcAn evaluated at time t and at sorption equilibrium (∞).

In figure 2.23, the kinetic curve of the desorption at concentration 100 ppm is not reported, because this process was performed at 15°C while the desorption at the other concentrations was conducted at 50°C. So, the desorption at 100 ppm is not comparable with desorption occurred for other concentrations. Anyway, the desorption kinetic curve of AcAn at concentration 100 ppm is reported in figure 2.24, together with the relative sorption curve.

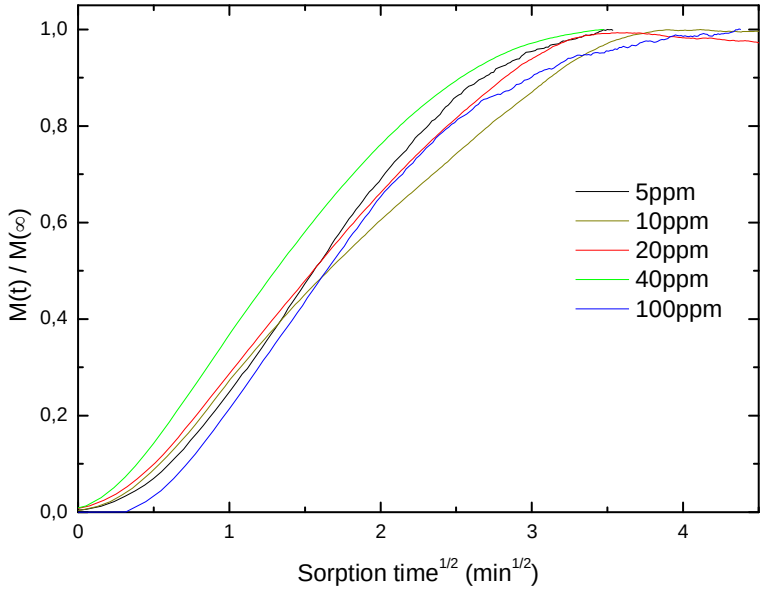

Figure 2.22 Sorption kinetic curves of different AcAn concentrations.

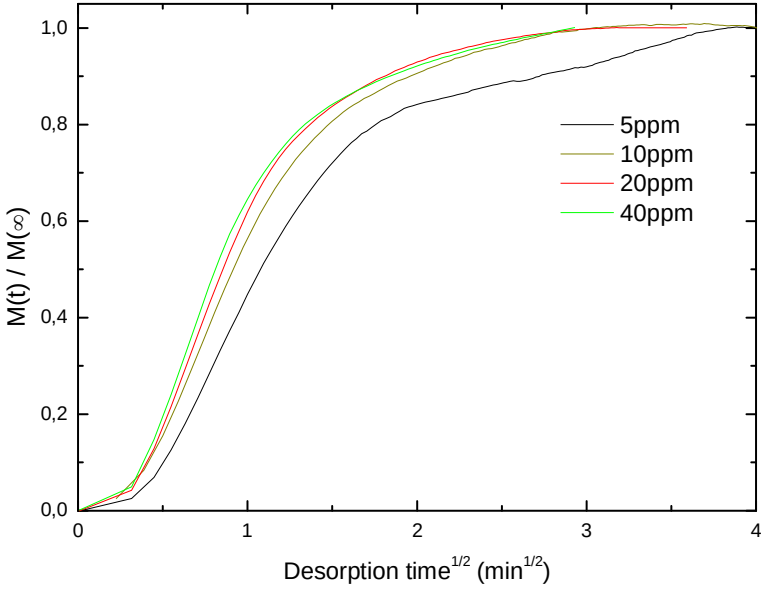

Figure 2.23 Desorption kinetic curves of different AcAn concentrations.

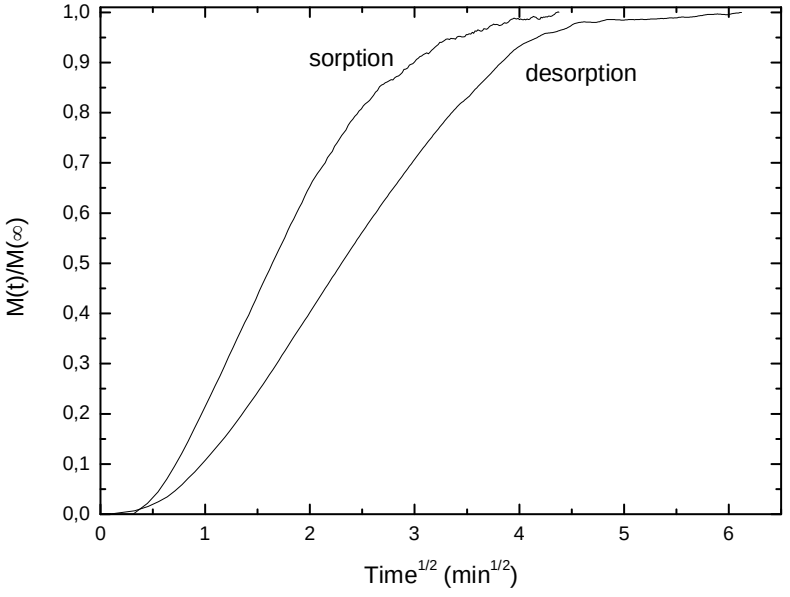

Figure 2.24 Sorption and desorption kinetic curves of AcAn at concentration 100 ppm.

As shown by the above curves, the sorption and desorption kinetics are only dependent on temperature and air flow rate, but not on the AcAn concentration in the inlet air. In fact, as already stated, for each value of AcAn concentration in inlet air the complete sorption happens in 16 minutes, and the desorption occurs in 5 minutes. However, varying temperature and air flow rate, you can affect the kinetics. During the sorption, in fact, a reduction of temperature and an increase in the inlet air flow lead to an enhancement in the amount and the kinetic of AcAn sorption. The desorption phase, instead, is faster by

increasing the temperature, and the concentration of AcAn in the outlet air increases by decreasing the outlet air flow rate.

The total amount of AcAn absorbed at equilibrium (and then also desorbed), starting from different concentrations of AcAn in the air flow, is reported in Table 2.3. Depending on the AcAn concentration in the inlet air, the beads of polymer inside the PCU are able to absorb from about 0.3 up to 2 mg of precursor.

Table 2.3. Amount of AcAn adsorbed at equilibrium for each starting concentration of AcAn.

AcAn initial concentration (ppm)	Total amount of AcAn absorbed (mg)
5	0.32
10	0.60
20	0.88
40	1.73
100	2.16

For every case tested, it is worth noting that the most part of the analyte amount is already absorbed within the polymer after a time lower than 16 minutes, and also the desorption time could be shorter than 5 minutes. For example, in the case of 5 ppm of AcAn in the inlet air, the 80% of AcAn is absorbed after 6 minutes, and always the

80% of AcAn is desorbed after 1 minute. So, significant amounts of AcAn can be also absorbed (and desorbed) in very short sorption/desorption cycles. As an example, starting from 5 ppm of AcAn in the air flow, after a cycle of 1 minute in sorption and 1 minute in desorption, the amount of AcAn released in the air is about 50 μg.

From the slopes of the sorption and desorption kinetic curves, considered in the range 0.5÷2 $min^{1/2}$, the diffusivity of AcAn in the crystalline phase of nanoporous δ sPS was also calculated using the following equation[37]:

$$\frac{M_{(t)}}{M_{(\infty)}} = 4\sqrt{\frac{D}{\pi \cdot R^2}}\sqrt{t}$$

where: M(t) is the mass of AcAn at any given time

M(∞) is the amount of AcAn absorbed at the equilibrium condition

D is the diffusivity

t is the time

R is the average sPS beads radius (~750 μm)

The values of the diffusivity so evaluated, both in sorption and desorption process, are reported in Table 2.4. It is noteworthy that the D values show a Fickian behaviour because they do not depend on the concentration of AcAn in the dilute mixture, so they can reasonably be taken as constant. Moreover, from the values in Table 2.4, the kinetics of desorption seem to be faster than the sorption

ones.

Table 2.4. Initial concentration and diffusivity constants for AcAn in sPS δ form at 15 °C (sorption) and 50 °C (desorption).

AcAn initial concentration (ppm)	D [cm^2/s] (sorption)	D [cm^2/s] (desorption)
5	$3.3\ 10^{-6}$	$0.8\ 10^{-5}$
10	$3.0\ 10^{-6}$	$1.0\ 10^{-5}$
20	$2.8\ 10^{-6}$	$1.3\ 10^{-5}$
40	$3.8\ 10^{-6}$	$1.5\ 10^{-5}$
100	$3.5\ 10^{-6}$	-

The values of D for all the AcAn concentrations tested were in the range $2.8 \div 3.8 \cdot 10^{-6}$ cm^2/sec for the sorption, while for the desorption D values range between 0.8 and $1.5 \cdot 10^{-5}$ cm^2/sec. The test at 100 ppm of AcAn has been performed at 15 °C, both in sorption and in desorption phase, to verify the correct estimation of diffusivity and the value of D for the desorption at this concentration of AcAn is in the range above mentioned[32,38].

2.7 The interfering agents question

As mentioned in the paragraph 1.2 of chapter 1, the two sensors that will be used in the CUSTOM device to detect drug precursors molecules are based on the LED-IF and the

LPAS techniques. These sensors could give false positive response because of the presence of some interfering molecules commonly present in the polluted air. LED-IF sensor is highly selective, based on specific recognition and then less sensitive towards interfering agents. LPAS sensor, instead, is more sensitive towards these agents because the detection of the drug precursor molecules is based on infrared wavelengths that can overlap with those ones of the interferents. In this regard, we can take advantage of the selectivity of the polymer towards certain types of molecules, allowing to narrow the range of wavelengths that could overlap with those ones of the precursors.

One of the CUSTOM project partner, the INSTM unit of the University of Modena and Reggio Emilia, has drawn up a list of selected wavelengths, through an elaborated statistical analysis started from the model reported by Webber[39], in order to minimize the wavelengths overlap of drug precursors with those of a selected list of interferents. Considering the environments in which the CUSTOM device will work and all the factors of air pollution, this INSTM unit suggested a list of more than 300 interfering species. Most of them were excluded by the list according to some considerations, such as if the interfering found in confined spaces is present in negligible amounts, and if the species

do not absorb light appreciably in the range of the LPAS laser and therefore do not interfere with the precursors, even if present in significant quantities.

On the basis of these considerations, the partners of the University of Modena and Reggio Emilia drew up the list of interfering agents (together with their maximum concentration found in the air) reported in Table 2.5.

Table 2.5 List of the possible interfering agents individuated by the partners of the INSTM unit of University of Modena and Reggio Emilia.

Air component molecule	**Maximum concentration [ppm]**
H_2O	60000
CO_2	1000
CH_4	10
CO	9
N_2O	1
NO_2	0.1
NO	0.1
O_3	0.1
SO_2	0.03
Interferent (gas)	**Upper limit [ppm]**
Butane	0.033
Ethylene	0.010
Propylene	0.010
1,3-butadiene	0.005

Interferent (liquid)	Upper limit [ppm]
Toluene	2.382
m, *p*-xylene	0.649
Ethylene glycol	0.491
Formaldehyde	0.400
Ethanol	0.146
Acetic acid	0.092
Naphthalene	0.071
Chloroform	0.038
Benzene	0.034
Ammonia	0.022
Methanol	0.016
o-xylene	0.016
Styrene	0.014
Acrylonitrile	0.011
Acrolein	0.011

Sorption and desorption tests in sPS nanoporous δ form samples with some of the listed interferents in gas phase, such as carbon dioxide, ethylene, propylene and 1,3-butadiene, have been performed and reported in literature[40-41]. The results show that these molecules are able to form clathrate structures with sPS nanoporous δ form, but their desorption kinetics, already happening at room temperature, are so fast that they can be considered

not stably absorbed in the polymer. This behavior is probably due to their too small molar volumes and a similar behavior can be expected also from the air component molecules.

Further sorption tests in sPS nanoporous δ form have been conducted with almost all the other interferents in liquid phase listed in Table 2.5. In these experiments, sPS nanoporous δ form aerogel samples were exposed to interferents vapours at 30°C for about 10 minutes, to ensure a high vapor pressure for each of them.

FTIR spectra of the sPS nanoporous δ form aerogel samples exposed to ethylene glycol and ammonia vapours are reported in figure 2.25 and 2.26, respectively.

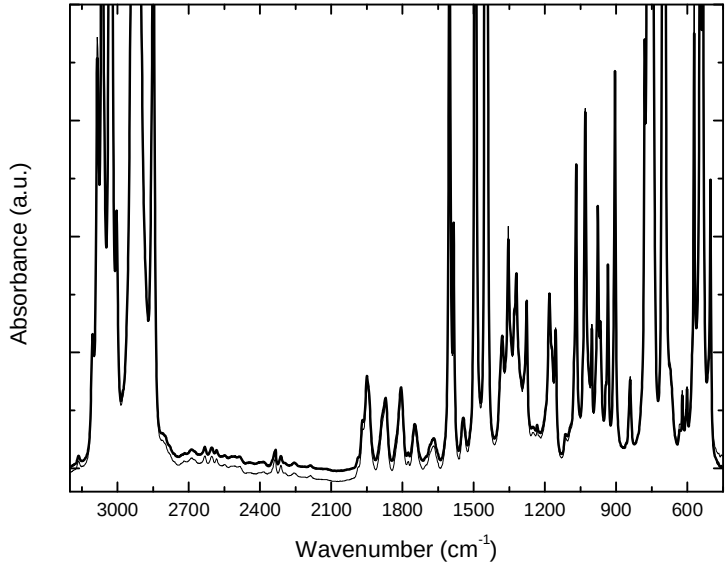

Figure 2.25 FTIR spectra of sPS nanoporous δ form aerogel before (thin line) and after (thick line) exposure to ethylene glycol vapours.

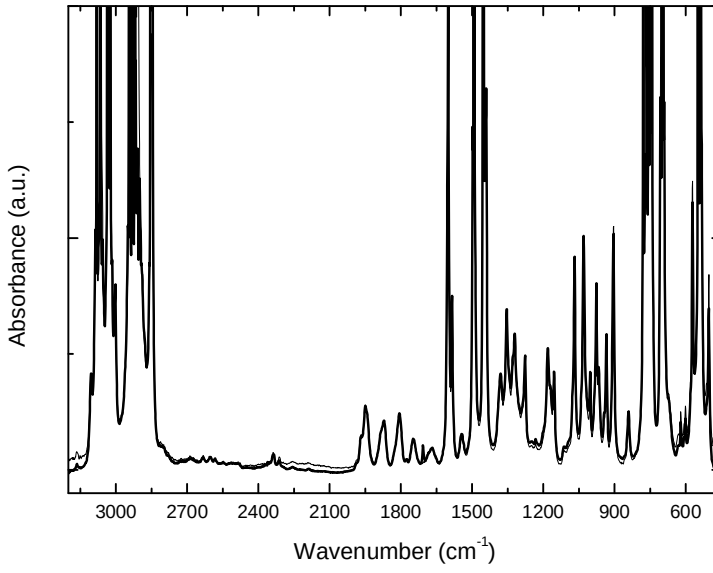

Figure 2.26 FTIR spectra of sPS nanoporous δ form aerogel before (thin line) and after (thick line) exposure to ammonia vapours.

The FTIR spectra shown above clearly indicate that neither ethylene glycol nor ammonia are absorbed in the polymer, not even in its amorphous phase.

In the figures from 2.27 to 2.31, the FTIR spectra of sPS nanoporous δ form aerogel samples exposed to the vapours of acetic acid, acrylonitrile, formaldehyde, ethanol and methanol are displayed. Where needed, some infrared bands are indicated with arrows for clarity.

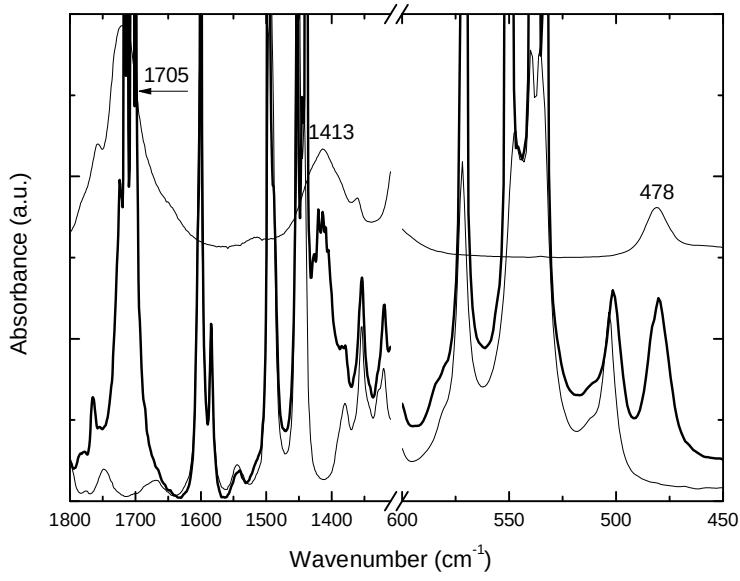

Figure 2.27 FTIR spectra of sPS nanoporous δ form aerogel (thin line, bottom), acetic acid absorbed in sPS nanoporous δ form aerogel (thick line) and pure acetic acid (thin line, top).

In the FTIR spectrum of the sPS nanoporous δ form aerogel sample exposed to acetic acid vapours (figure 2.27), all the typical intense infrared bands of this interferent, e.g. those at 1705, 1413 and 478 cm^{-1} labelled in figure, are present. It is worth noting that in this FTIR spectrum, as well as in others that will follow, are shown only the regions of wavelengths in which the most intense absorbance bands of the interferents are present. By TGA measurements, the amount of acetic acid in the polymer is about 5% by weight.

Also in the FTIR spectrum of the polymer sample exposed

to acrylonitrile vapours, in figure 2.28, its typical infrared bands at 2233, 1654, 1411, 1095 and 970 cm^{-1} are present, accounting for an amount of acrylonitrile in the polymer of 25% by weight.

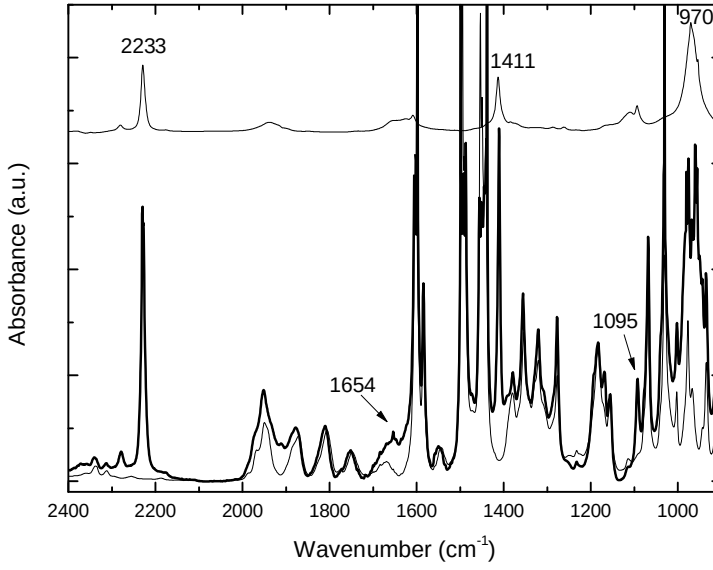

Figure 2.28 FTIR spectra of sPS nanoporous δ form aerogel (thin line, bottom), acrylonitrile absorbed in sPS nanoporous δ form aerogel (thick line) and pure acrylonitrile (thin line, top).

In figure 2.29, the FTIR spectra of sPS nanoporous δ form before and after the exposure to formaldehyde vapours are reported. In the spectrum of the polymer sample exposed to formaldehyde vapours are labelled the characteristic absorbance bands of this interfering agent, i.e. those at 3572, 1126 and 1099 cm^{-1}. Its quantity within the sPS nanoporous δ form aerogel sample resulted to be 11% by

TGA measurements.

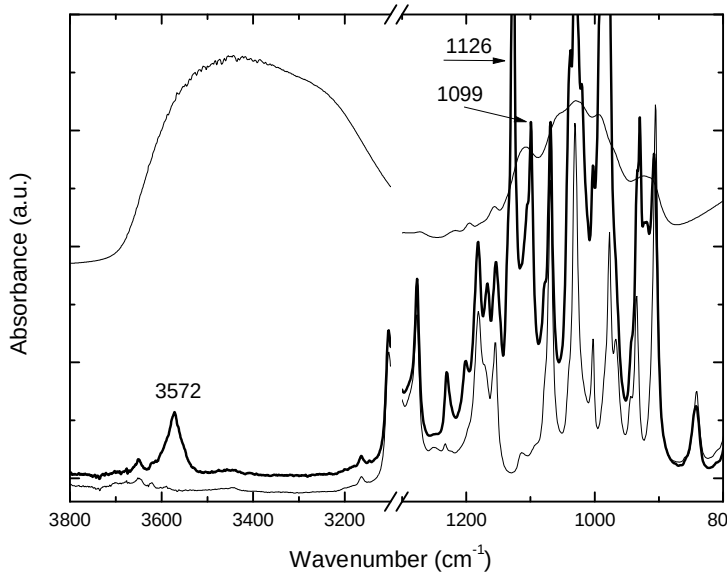

Figure 2.29 FTIR spectra of sPS nanoporous δ form aerogel (thin line, bottom), formaldehyde absorbed in sPS nanoporous δ form aerogel (thick line) and pure formaldehyde (thin line, top).

In figure 2.30, the FTIR spectrum of a polymer aerogel sample exposed to ethanol vapours is reported, together with the values of the typical infrared bands of ethanol at 3619-3127, 1090 and 879, cm^{-1}. The quantity of ethanol absorbed by the polymer is around 22%.

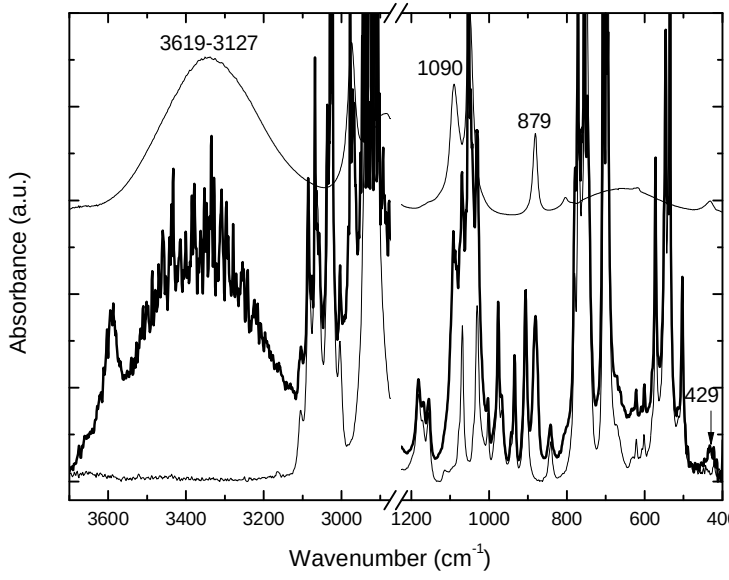

Figure 2.30 FTIR spectra of sPS nanoporous δ form aerogel (thin line, bottom), ethanol absorbed in sPS nanoporous δ form aerogel (thick line) and pure ethanol (thin line, top).

The FTIR spectrum of a sPS nanoporous δ form aerogel sample exposed to methanol vapours is reported in figure 2.31, where the most intense methanol infrared bands, at 3613-3124 and 1021 cm^{-1}, are shown. The polymer sample exposed to methanol vapours has absorbed around 32% of this interferent, as resulted by TGA.

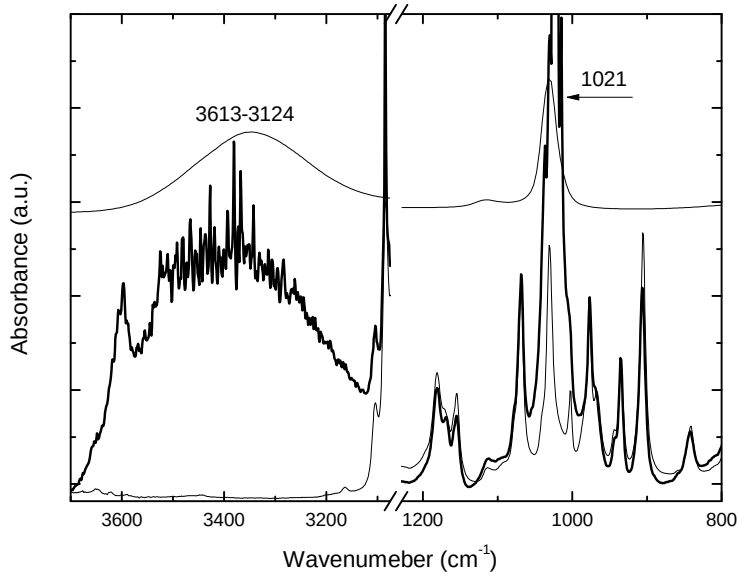

Figure 2.31 FTIR spectra of sPS nanoporous δ form aerogel (thin line, bottom), methanol absorbed in sPS nanoporous δ form aerogel (thick line) and pure methanol (thin line, top).

Even if the interfering molecules examined so far are absorbed in the polymer, not all are absorbed in the crystalline cavities of the sPS nanoporous δ form. The X-ray diffraction patterns shown in figure 2.32 illustrate that only acrylonitrile, acetic acid and formaldehyde form cocrystalline structures with the polymer. In these cases, in fact, the increasing of the intensity reflection at $2\theta = 10.2°$ and the reduction of those ones at $2\theta = 8.2°$ and $13.6°$ clearly show the occurred clathration; while ethanol and methanol sorptions do not involve modifications in the

crystalline pattern, so they will be not concentrated by the crystalline phase of the polymer. Most probably, ethanol and methanol are only absorbed by the amorphous phase of sPS.

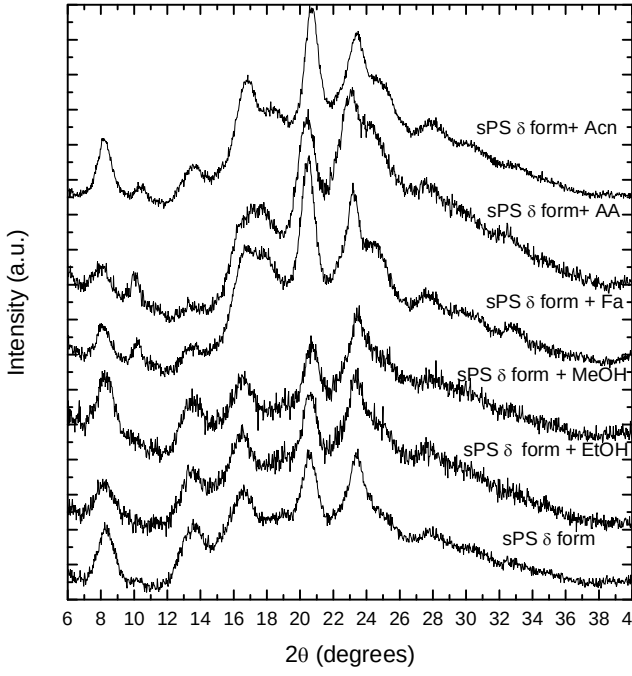

Figure 2.32 WAXD spectra of sPS nanoporous δ form aerogel samples exposed to vapours of: ethanol (EtOH), methanol (MeOH), formaldehyde (Fa), acetic acid (AA) and acrylonitrile (Acn).

Among the species listed in Table 2.5 as liquid interferent, there are in particular 3 molecules whose absorbance bands have shown, during the simulation tests performed by INSTM unit of Modena and Reggio Emilia, the most

overlap with those of the target precursors. In order to verify if the sorption of such interferents influences the concentration factor of the precursors within the polymer, some tests have been performed on sPS nanoporous δ form aerogel samples exposed to mixtures of such interferents with a drug precursor. The precursor chosen was BMK and the interferents tested in mixture with it were chloroform ($CHCl_3$), *p*-xylene (*p*-xy) and naphthalene (naph). Moreover, even if DCE is not present among the interferents in Table 2.5, we also performed tests on a polymer sample dipped in a mixture of DCE and BMK, because DCE is a very common and persistent pollutant in the air. All the tests have been conducted on mixtures BMK/interferent in concentrations ratio 10/1, prepared considering that the concentrations of interfering agents usually observed in the environment are less than 1 ppm. The experiments have been performed immerging sPS nanoporous δ form aerogel samples in aqueous solutions containing the mixtures above mentioned. On these samples were then carried out FTIR and WAXD measurements, whose spectra are shown in the following figures.

In figure 2.33, the FTIR spectrum of the aerogel sample exposed to the mixture BMK/$CHCl_3$ in ratio 10/1 is reported. For the sake of comparison, the FTIR spectra of

pure BMK, pure $CHCl_3$ and pure sPS nanoporous δ form are also shown. The absorbance bands at 1715 and 1214 cm^{-1}, labeled in the figure, are related to BMK and $CHCl_3$ respectively. The infrared absorbance band at 1715 cm^{-1} could be attributed also to the $CHCl_3$, but the intensity of this band is the same of that one observed in the FTIR spectrum of the aerogel sample exposed to 10ppm aqueous solution of BMK (see figure 2.6). The *cf* of $CHCl_3$ in the mixture is $1{\cdot}10^3$, so it has been concentrated even more than BMK, whose *cf* is $4{\cdot}10^2$, but the precursor *cf* is not affected by the presence of this interferent because it is the same as if the BMK is alone in 10ppm aqueous solution[42].

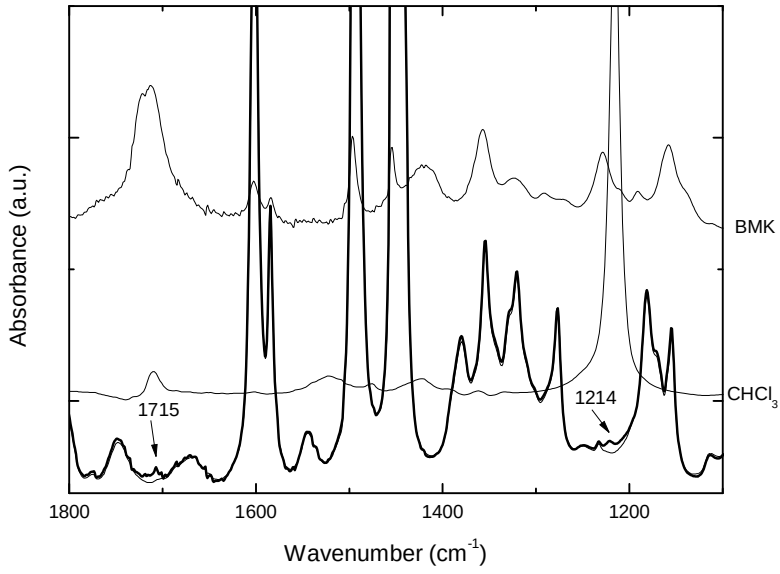

Figure 2.33 FTIR spectra of sPS nanoporous δ form aerogel sample exposed to the aqueous solution mixture BMK/$CHCl_3$ in ratio 10/1 (thick line). Pure BMK and $CHCl_3$ FTIR spectra (thin lines, top) are also reported for comparison, together with pure sPS FTIR spectrum (thin line, bottom).

In figure 2.34, the FTIR spectrum of the polymer sample exposed to the mixture 10/1 of BMK/*p*-xylene is reported. Also here, for comparison the FTIR spectra of pure BMK, pure *p*-xylene and pure sPS nanoporous δ form aerogel are reported. The absorbance band relative to BMK presence is that at 1715 cm^{-1}, while the infrared absorbance bands at 1515, 1219, 1119, 798 and 484 cm^{-1}, labeled in the figure with arrows, are related to the presence of *p*-xylene. This interferent has been concentrated within the polymer,

as confirmed by its *cf* in the mixture that is $4 \cdot 10^4$. Also the BMK was concentrated with a *cf* close to $4 \cdot 10^2$ and, even if sPS is more selective towards *p*-xylene than towards BMK, the uptake of the precursor is not influenced by the presence of the interferent, because the *cf* of BMK from 10ppm aqueous solution remains unaltered[42].

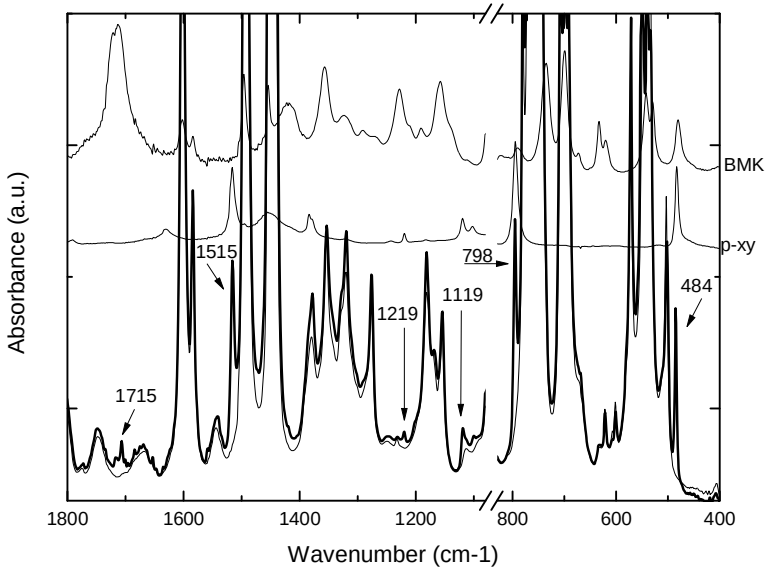

Figure 2.34 FTIR spectra of sPS nanoporous δ form aerogel sample exposed to the aqueous solution mixture BMK/p-xy in ratio 10/1 (thick line). Pure BMK and *p*-xylene FTIR spectra (thin lines, top) are also reported for comparison, together with pure sPS FTIR spectrum (thin line, bottom).

In figure 2.35, the FTIR spectrum of the polymer sample exposed to the mixture BMK/naphthalene is shown, together with the FTIR spectra of pure BMK, pure

naphthalene and pure sPS nanoporous δ form aerogel, reported for comparison. The absorbance bands, labeled with arrows, are those relative to the interferent at 1210, 1124 and 478 cm^{-1}, and that one relative to BMK presence at 1715 cm^{-1}. Once again, both the interferent and the precursor have been concentrated within the sPS, with *cf* that are $4 \cdot 10^4$ and $4 \cdot 10^2$, respectively. The polymer is selective towards naphthalene, but the *cf* of the BMK is not affected by its presence[42].

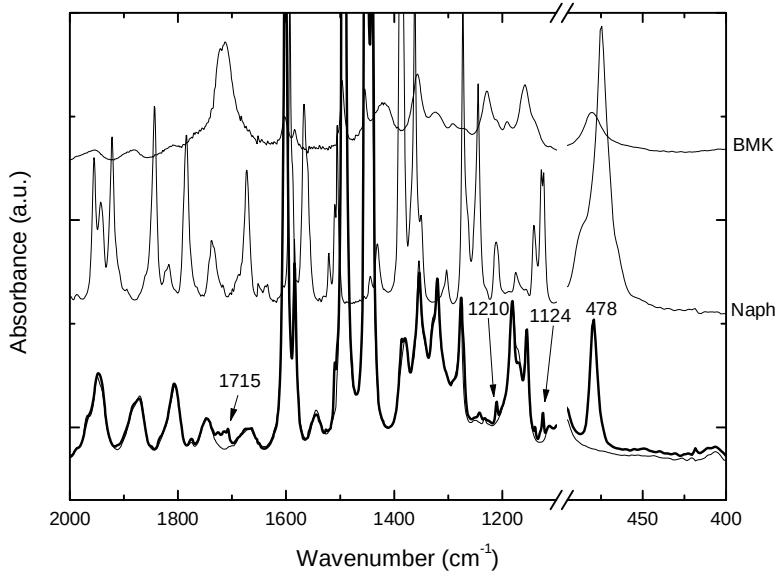

Figure 2.35 FTIR spectra of sPS nanoporous δ form aerogel sample exposed to the aqueous solution mixture BMK/naph in ratio 10/1 (thick line). Pure BMK and naphthalene FTIR spectra (thin lines, top) are also reported for comparison, together with pure sPS FTIR spectrum (thin line, bottom).

In figure 2.36, the FTIR spectrum of the polymer sample exposed to the mixture BMK/DCE is shown, as well as the FTIR spectra of pure BMK, pure DCE and pure sPS nanoporous δ form aerogel for comparison. The absorbance band at 1715 cm^{-1} and 1235 cm^{-1}, labeled with arrows, are the most intense bands of BMK and DCE, respectively. The c*f* of DCE is around $4 \cdot 10^4$ while the *cf* of BMK remains about $4 \cdot 10^2$, so even if sPS is selective towards DCE, the uptake of BMK is not affected by the presence of DCE.

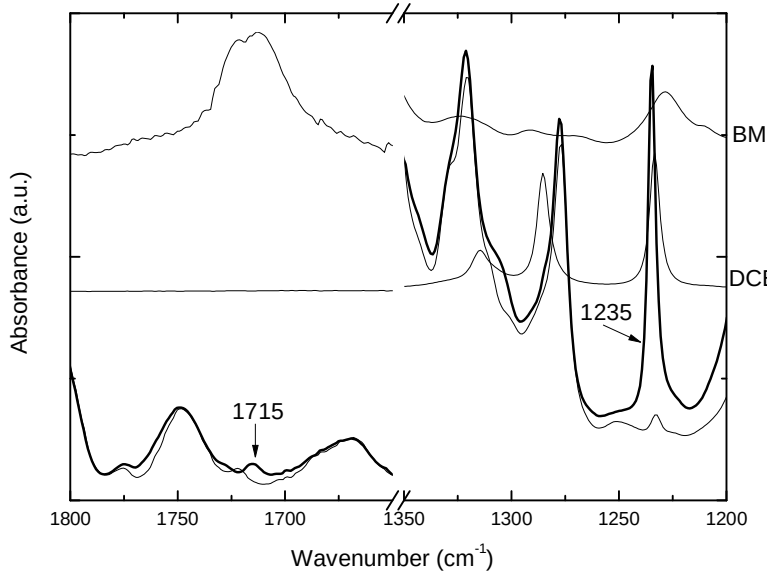

Figure 2.36 FTIR spectra of sPS nanoporous δ form aerogel sample exposed to the aqueous solution mixture BMK/DCE in ratio 10/1 (thick line). Pure BMK and DCE FTIR spectra (thin lines, top) are also reported for comparison, together with pure sPS FTIR spectrum (thin line, bottom).

The WAXD spectra of the aerogel samples exposed to mixture of BMK and interferents are reported in figure 2.37. In the figure, you can see that only aerogel samples exposed to the mixtures BMK/p-xy, BMK/naph and BMK/DCE in ratio 10/1 show WAXD pattern typical of cocrystalline structures. It is likely that the clathrate formation is due to the presence of such interferents, rather than to the presence of BMK, because the WAXD spectrum of an aerogel sample exposed to BMK aqueous solution 10ppm (see figure 2.7) does not show the typical pattern of a cocrystal. Regarding the WAXD spectrum of the mixture BMK/$CHCl_3$, it does not show neither an increase for the reflection at 2θ=10.2°, nor a reduction in the intensity of the reflections at 2θ=8.2 and 13.6°, unlike the other WAXD patterns in the same figure. The amounts of interferent molecules in the cavities of the sPS crystal lattice are quite high in the case of naph (14%), p-xy (17%) and DCE (20%), while the $CHCl_3$ occupies just 1% of these crystalline cavities. Then, the amount of $CHCl_3$ in the cavities of the sPS crystal lattice is not enough to visualize the pattern of the clathrate structure through X-ray diffraction.

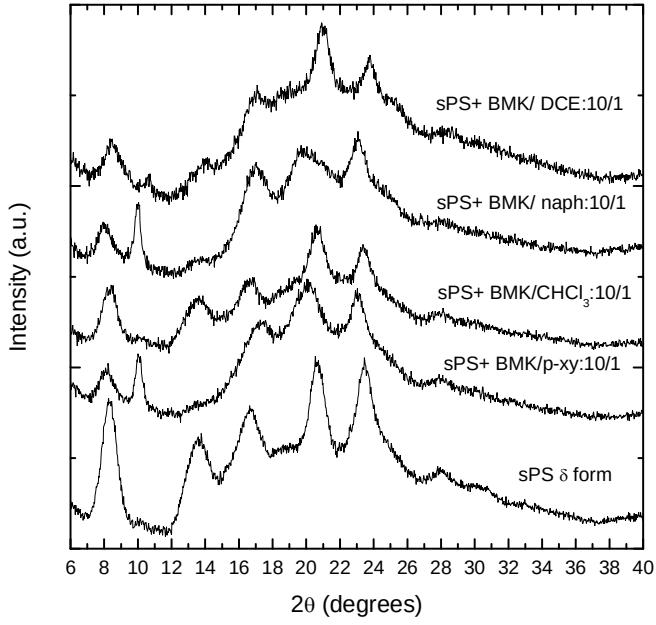

Figure 2.37 WAXD spectra of sPS nanoporous δ form aerogel samples exposed to different aqueous solutions mixtures BMK/interferent in ratio 10/1. Pure sPS nanoporous δ form WAXD spectrum is also reported for comparison.

In summary, about 2/3 of the interferents in Table 2.5 do not form co-crystalline structures with sPS nanoporous δ form and so they are not concentrated by the crystalline phase of the polymer. Only about 10 species, on the almost 30 listed in the table, are able to form cocrystals with the polymer and therefore can be considered as real interferents. Moreover, it could exist a connection between the selectivity of sPS nanoporous δ form and Hansen's solubility parameter of the molecules forming or not

cocrystalline structure. Anyway, it is a matter of fact that molecules forming clathrate structures with sPS nanoporous δ form have a solubility parameter close to that one of the polymer, which is 9.3 $(cal\ cm^{-3})^{1/2}$. For example, the solubility parameters of the just mentioned p-xylene and naphthalene are 8.8 and 9.9 $(cal\ cm^{-3})^{1/2}$ respectively, very close to the solubility parameter value for sPS.

In order to further understand the selectivity mechanism of sPS nanoporous δ form, we performed some experiments in aqueous solutions containing a mixing of 3 ppm of interfering molecules, such as $CHCl_3$, DCE and *p*-xy, in ratio 1/1. The aqueous solutions prepared were: $CHCl_3$/DCE, $CHCl_3$/*p*-xy and DCE/*p*-xy.

The FTIR spectra of the polymer samples treated as above mentioned are shown below.

The FTIR spectrum of the polymer sample exposed to the mixture $CHCl_3$/DCE is shown in figure 2.38, where the FTIR spectra of pure $CHCl_3$, DCE and sPS nanoporous δ form aerogel are also reported for comparison. In the FTIR spectrum of the polymer sample immersed in the aqueous solution is present only the absorbance band at 1235 cm^{-1}, characteristic of DCE, whose c*f* is around $2 \cdot 10^4$.

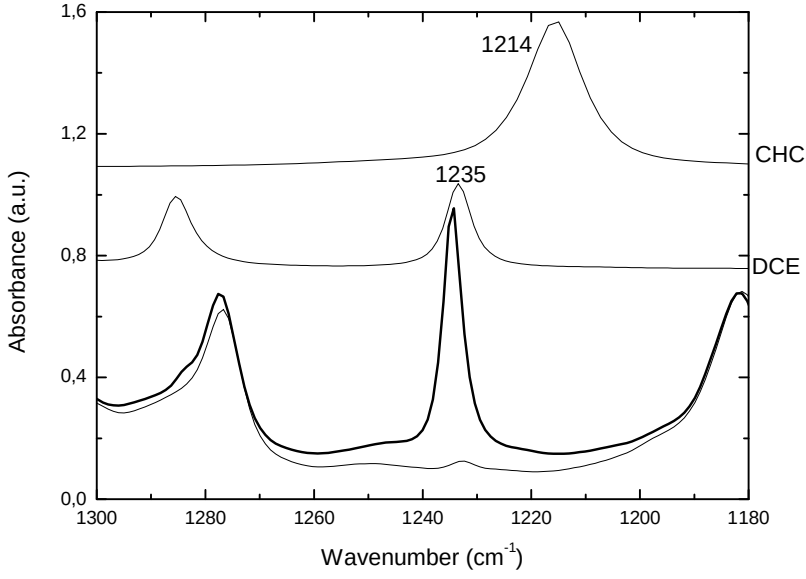

Figure 2.38 FTIR spectra of sPS nanoporous δ form aerogel sample exposed to the aqueous solution mixture $CHCl_3$/DCE in ratio 1/1 (thick line). Pure $CHCl_3$ and DCE FTIR spectra (thin lines, top) are also reported for comparison, together with pure sPS FTIR spectrum (thin line, bottom).

In figure 2.39, the FTIR spectra of the sPS nanoporous δ form aerogel sample exposed to the mixture $CHCl_3$/*p*-xy, and those of pure $CHCl_3$, *p*-xy and sPS are reported. In the FTIR spectrum of the polymer sample immersed in the aqueous solution, you find only the presence of the *p*-xy absorbance bands at 1219 and 1515 cm^{-1}. The c*f* of *p*-xy in this solution is around $3 \cdot 10^4$.

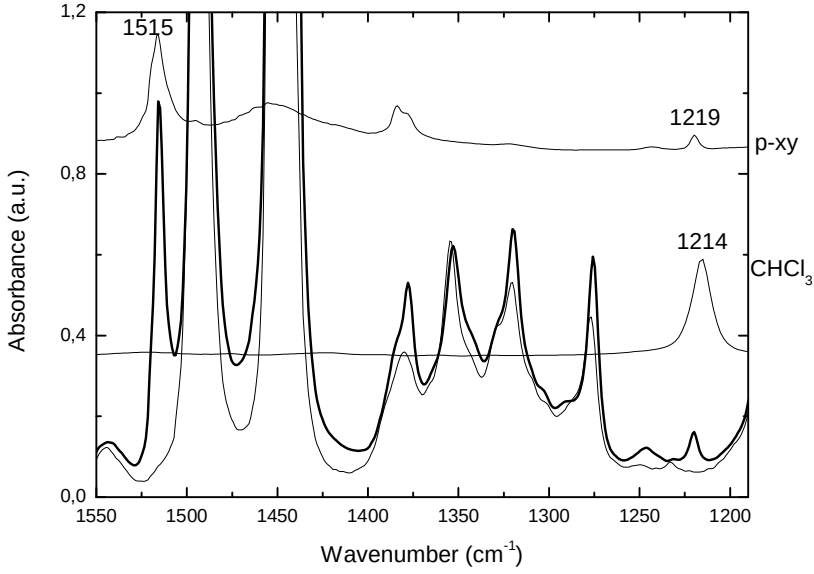

Figure 2.39 FTIR spectra of sPS nanoporous δ form aerogel sample exposed to the aqueous solution mixture $CHCl_3$/*p*-xy in ratio 1/1 (thick line). Pure $CHCl_3$ and *p*-xy FTIR spectra (thin lines, top) are also reported for comparison, together with pure sPS FTIR spectrum (thin line, bottom).

In figure 2.40, the FTIR spectra of the polymer sample treated with the solution DCE/*p*-xy is reported, together with the FTIR spectra of the pure DCE, *p*-xy and sPS for comparison. Here, the presence of both molecules in the sample is confirmed by the presence of the absorbance bands at 1235 cm^{-1}, for DCE, and at 1515 and 1219 cm^{-1} for *p*-xy. The *cf* for DCE, in this case, is $1 \cdot 10^4$ and $2 \cdot 10^4$ for *p*-xy.

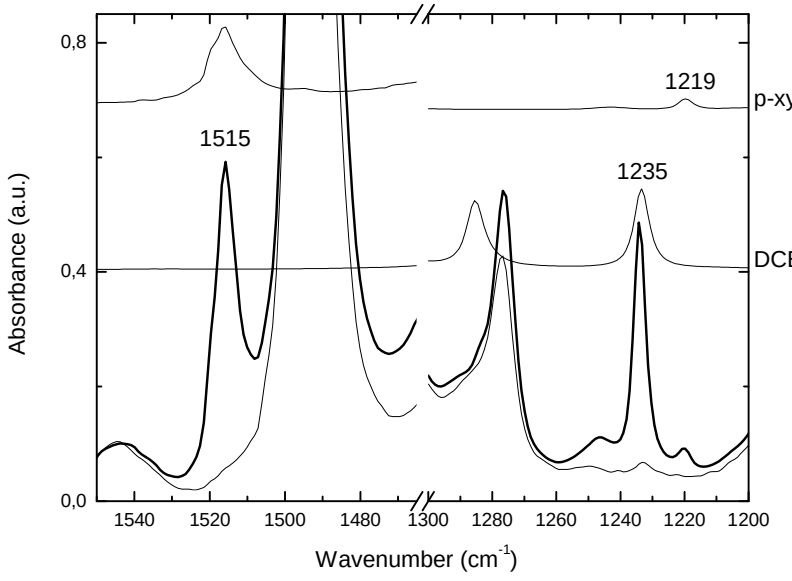

Figure 2.40 FTIR spectra of sPS nanoporous δ form aerogel sample exposed to the aqueous solution mixture DCE/*p*-xy in ratio 1/1 (thick line). Pure DCE and *p*-xy FTIR spectra (thin lines, top) are also reported for comparison, together with pure sPS FTIR spectrum (thin line, bottom).

From these experiments, it is clear that nanoporous sPS δ form aerogel is selective towards DCE and pXy. DCE and pXy *cf* into the polymer remain substantially unchanged if they are exposed to a mixture containing one of them together with $CHCl_3$, but also if the polymer is exposed to a 1/1 mixture of these two VOCs.

Chapter 3

Experimental part

3.1 Materials and techniques

The syndiotactic polystyrene used for all the experiments was manufactured by Dow Chemicals under the trademark Questra 101. ^{13}C nuclear magnetic resonance characterization showed that the content of syndiotactic triads was over 97%.The mass average molar mass obtained by gel permeation chromatography in trichlorobenzene at 135°C was found to be $Mw=3.2\cdot10^5$ g mol^{-1} with a polydispersity index Mw/Mn=3.9.

All the solvents were purchased from Aldrich and used without further purification.

Aerogel samples were obtained by treating native gels with a SFX 200 supercritical carbon dioxide extractor (ISCO Inc.) using the following conditions: T=40°C, P=200 bar, extraction time t=180 min.

The infrared absorbance spectra were obtained at a resolution of 2.0 cm^{-1} with a Bruker Vertex70 spectrometer, equipped with deuterated triglycine sulfate (DTGS) detector and a KBr beam splitter. The frequency scale was internally calibrated to 0.01 cm^{-1} using a He-Ne laser and 32 scans were signal averaged to reduce the noise. The FTIR spectra shown in the previous chapter are

mostly in the wavenumbers range 1800-400 cm^{-1}, because in this range the main absorbance bands of the polymer and the precursors are present.

The X-rays diffraction patterns were obtained on a Bruker D8 automatic diffractometer operating with nickel-filtered Cu Kα radiation.

The thermogravimetric measurements were performed with a TG 209 F1 from Netzsch in nitrogen flow at 10 mL/min and heating speed of 10 K/min.

Mass spectrometer measurements were performed with an on-line quadrupole mass detector Trace MS by ThermoQuest.

Scanning electron micrographs were obtained using an ASSING LEO scanning electron microscope.

Surface area values were obtained by N_2 adsorption measurements carried out at 77K on a Micromeritics ASAP 2020 sorption analyzer.

3.2 Procedure for the preparation of beads of sPS nanoporous δ form aerogel

The beads of sPS nanoporous δ form aerogel were prepared as follows. A solution of sPS in chloroform, at 10% by weight of the polymer (typically 1.48 g of sPS in 10 mL of solvent), was heated at 110°C up to the complete dissolution of the polymer. The solution of the polymer was

transferred still warm into a fluid dispenser (Dispenser KW-4AD supplied by Chemat Technology, Inc.), a sort of syringe which allows a regular dropping at controlled rate. An impulse every 10 seconds was send to the dispenser and the drops were ejected, falling in a beaker with diethyl ether held at -80°C thanks to the dry ice bath where it was placed. In this way, the drops of polymer solution coagulate in diethyl ether forming gels with bead shapes.

These last are converted in the corresponding aerogels by extraction with carbon dioxide in supercritical conditions.

Conveniently, in carrying out sorption/desorption tests of drug precursors we used thin slices of sPS nanoporous δ form aerogels, obtained by cutting with a scalpel a cylindrical shaped gel then extracted as above mentioned.

3.3 Degree of crystallinity

The degree of crystallinity of sPS nanoporous δ form aerogel samples has been evaluate both from their FTIR and WAXD spectra.

By subtracting out the amorphous phase contribution from FTIR spectra of sPS nanoporous δ form aerogel samples, we obtained a straightforward isolation of the spectra of the sPS crystalline phases and the quantitative determination of the crystalline and amorphous content. The infrared based degree of crystallinity, expressed as

weight fraction X_c, has been evaluated according to the equation:

$$K = \frac{l}{l'} \cdot (1 - X_c)$$

where: K is the subtraction coefficient

l is the thickness of the sample

l' is the thickness of an amorphous reference sample.

The ratio l/l' is estimated from the absorbance ratio of a conformationally insensitive peak. The spectral subtraction was achieved by reducing the peak at 1379 cm^{-1}, prevailingly associated to the amorphous phase and so the most suitable for crystallinity evaluation, to the baseline[43-44].

The degree of crystallinity based on WAXD spectra has been determined by using the classical method of Hermans and Weidinger[45]. The diffraction pattern has been resolved into two areas, A_c and A_a, that are proportional to the crystalline and amorphous weight fractions, respectively. Then, the degree of crystallinity has been calculated through the expression:

$$X_c = \frac{A_c}{A_c + A_a} \cdot 100$$

3.4 Porosity evaluation of beads of sPS nanoporous δ form aerogel

The porosity (P) of the beads of sPS nanoporous δ form aerogel has been evaluated through the following equation[1]:

$$P = 100 \cdot (1 - \frac{\rho}{\rho_s})$$

where: ρ is the aerogel apparent density (calculated from the mass/volume ratio of the aerogel)

ρ_s is the density of the polymer matrix (equal to 1.02 g/cm^3 for a semicrystalline sPS δ form with a degree of crystallinity near to 40%)

3.5 Procedure for the preparation of aqueous solutions at different concentrations

The sorption experiments of BMK and safrole within the polymer have been performed by aqueous solutions at different concentrations. The aqueous solutions have been prepared dissolving a certain amount of precursor (depending on the desired concentration) in 3 L of distilled water. Then, a sPS nanoporous δ form aerogel sample has been immersed in the solution and stirred at room temperature for about 24 hours, to be sure that the equilibrium condition would be reached. For the mixtures between BMK and the interferents, both species have

been dissolved in distilled water in the same conditions above mentioned.

3.6 Procedure for building calibration lines and equilibrium uptake curves

To evaluate the drug precursor equilibrium uptake values in the polymer, calibration lines were previously built. In the calibration lines it was reported the intensity of an infrared band of the absorbed drug precursor, normalized with respect to a polymer band independent from the degree of crystallinity, versus the weight percent of the precursor absorbed by the polymer valued by TGA. For the safrole, the band of the precursor is that at 1640 cm^{-1} and it is normalized respect to the band of sPS at 1584 cm^{-1}. For BMK two calibration lines have been built: one for the highest concentrations of the precursor (500 and 250 ppm) and another for the lowest ones (100, 50, 10 and 1 ppm). In the former case the intensity of the absorbance band of BMK at 1715 cm^{-1} has been normalized to the band of sPS at 1584 cm^{-1}; in the latter, the band of BMK at 1229 cm^{-1} was normalized to the absorbance band of sPS at 1276 cm^{-1}. So, thanks to these curves, it was possible to know the amount of guest precursor absorbed into the polymer at any concentration by using only the FTIR measurements.

The calibration line for the AcAn has been built reporting the intensity of the signal m/z=43 (the most intense for AcAn), given by the mass spectrometer, vs the concentration of AcAn in ppm.
The equilibrium uptake curves have been built reporting the amount of precursors absorbed, obtained through the calibration lines, vs the concentration in ppm.

3.7 Procedure to obtain the desired AcAn concentration in the air flow

For the sorption experiments of AcAn within the beads of polymer (sPS aerogel amount loaded in the PCU=350 mg), we used the homemade experimental apparatus described in figure 2.17, capable to produce an air flow containing the precursor in low concentration. The well-defined concentration of AcAn in the air flow is calculated starting from the Raoult's law

$$P\, y_j = P^0\, x_j$$

where: P is the total pressure (equal to 1 atm)

y_j is the molar fraction of AcAn in vapour phase

P^0 is the vapour pressure of AcAn

x_j is the molar fraction of the pure liquid (equal to

1 because AcAn is the only liquid in the system)

So, we can write (putting j = AA, i.e. acetic anhydride):

$$1\ y_{AA} = P_{AA}^{0}\ 1$$

Explaining the molar fraction of AcAn (AA):

$$y_{AA} = \frac{Q_{AA}}{Q_{AA} + Q_{air}}$$

where Q is the mass flow.

Since Q_{air} >> Q_{AA} we can write:

$$y_{AA} = \frac{Q_{AA}}{Q_{air}} = P_{AA}^{0}$$

From the last equation we can obtain Q_{AA} and Q_{air}, corresponding to the percentage of air that must pass through the MFCs to get the desired concentration of AcAn in the air flow.

We can get Q_{air} knowing Q_{AA} and P_{AA}^{0}. Q_{AA} is obtained from:

$$Q_{AA} = Q_{tot}.C_{AA}$$

where Q_{tot} is the total mass flow of the used MFC and C_{AA} is the concentration of AcAn. Both these values are known because they are chosen by the operator.

P_{AA}^{0} is derived from Antoine's law:

$$log_{10}P_{AA}^{0} = A - \frac{B}{C + T}$$

in which T is the temperature and A, B and C (respectively 7.12160, 1427.770, 198.050) are constants obtained experimentally.[46]

The response of MS at a certain mass flow was calibrated entering different concentrations of AcAn and recording the MS signal intensity of the characteristic AcAn peak at m/z=43. The instrument response is linear in the range of concentrations considered. For each different air flow used during the tests, a calibration has been made.

Chapter 4
Conclusions

In this thesis we dealt with the preparation and characterization of the beads of sPS nanoporous δ form aerogel, as well as the capacity and the effectiveness of this polymer to absorb the most common and dangerous drug precursors on the market: benzyl methyl ketone (BMK), ephedrine (Eph), safrole and acetic anhydride (AcAn). Moreover, we validated the working operation of the preconcentrator unit (PCU), realized by ENEA for the CUSTOM project, in order to concentrate drug precursors during the sampling then send to the sensors of the CUSTOM device. Finally, we tested the influence of some interfering agents on the sorption of the target precursors.

The first challenge faced in this work has been the preparation of the beads of sPS nanoporous δ form aerogel. We achieved these beads developing a suitable procedure, after many attempts with different pairs of solvents/non-solvents and at different polymer concentrations, that guarantees quite regular shape (about spherical) and small dimensions (between 0.1 and 1 mm).

The sPS nanoporous δ form aerogel was demonstrated to be suitable for the sorption of three drug precursors at very low activity, and so for the CUSTOM project aims, because

it ensures high concentration factors (1 10^4 for BMK, 5 10^4 for Safrole, 2 10^2 for AcAn; higher than those obtainable with other absorbing materials, i.e. activated carbon) and presents fast sorption and desorption kinetics.

Moreover, we validated the operation mode of the PCU, i.e. how it held temperature, pressure and the air flow set. Furthermore, in laboratory tests, we proved that PCU effectively concentrates at least one of the target precursors, AcAn, also in short sorption/desorption cycles.

With AcAn, studies on the sorption and desorption kinetics and on diffusivity in the polymer have been also conducted. The results obtained show that the sorption and desorption kinetics are fast, and in particular those of the desorption are faster than the sorption ones.

Another thorny problem we had to face was represented by the interfering agents, commonly present in polluted air, possibly absorbed by the polymer. The presence of such interferents could be a serious problem for the sensors of the device, especially for LPAS, whose detection method of drug precursors is based on infrared wavelengths, which can overlap with those ones of the interferents giving a false positive response. In this regard, we took advantage from the selectivity of the polymer towards certain kinds of molecules to narrow the field of possible interfering agents. In fact, from the initial list of about 30 possible interferents

drawn by one of the CUSTOM project partner, only about 10 can be concentrated by the sPS nanoporous δ form aerogel; moreover, in the PCU the polymer effectively absorbs precursors with an unchanged concentration factor even in presence of interferents, i.e. in environmental conditions very similar to those that presumably occur in real use circumstances of the CUSTOM device (e.g. in customs, airports, railways).

The sPS nanoporous δ form aerogel has proven to be an effective material in absorb and concentrate the target drug precursors molecules, even when they are in very low concentrations. This behaviour of the polymer, together with a good selectivity towards some kind of molecules, has made it the most suitable material for the purposes of the CUSTOM project.

References

(1) Daniel, C.; Sannino, D.; Guerra, G. *Chem. Mater.* 2008, *20*, 577.

(2) Venditto, V.; De Girolamo Del Mauro, A.; Mensitieri, G.; Milano, G.; Musto, P.; Rizzo, P.; Guerra, G. *Chem. Mater.* 2006, *18*, 2205.

(3) United Nations Convention against illicit traffic in narcotic drugs and psychotropic substances.United Nations. 1988.

(4) Regulation (EC) No 273/2004

(5) Precursors and chemicals frequently used in the manufacture of narcotic drugs and psychotropic substances. Annual report 2009.

(6) World Drug Report 2010. United Nations Office on Drugs and Crime.

(7) Jackwerth, E.; Mizuike, A.; Zolotov, Y. A.; Berndt, H.; Hohn, R.; Kuzmin, N. M. *Pure & Appl. Chem.* 1979, *51*, 1195.

(8) Gallego, M.; Peiia, Y. P. D.; Valcrcel, M. *Analytical Chemistry* 1994, *66*, 4074.

(9) Trammell, S. A.; Zeinali, M.; Melde, B. J.; Charles, P. T.; Velez, F. L.; Dinderman, M. A.; Kusterbeck, A.; Markowitz, M. A. *Analytical Chemistry* 2008, *80*, 4627.

(10) Gedrich, K.; Senkovska, I.; Klein, N.; Stoeck,

U.; Henschel, A.; Lohe, M. R.; Baburin, I. A.; Mueller, U.; Kaskel, S. *Angewandte Chemie (International ed. in English)* 2010, *49*, 8489.

(11) Pinalli, R.; Barboza, T.; Bianchi, F.; Massera, C.; Ugozzoli, F.; Dalcanale, E. *Supramolecular Chemistry* 2013, *DOI:10.1080/10610278.2013.814778*.

(12) Pereira Nascimento Filho, A.; Tressino De Carvalho, A.; Pereira da Silva, M. L.; Demarquette, N. R. *Materials Research* 2006, *9*, 33.

(13) Chen, X.; Hu, L.; Liu, J.; Chen, S.; Wang, J. *TrAC Trends in Analytical Chemistry* 2013, *48*, 30.

(14) Milano, G.; Venditto, V.; Guerra, G.; Cavallo, L.; Ciambelli, P.; Sannino, D. *Chem. Mater.* 2001, *13*, 1506.

(15) Daniel, C.; Longo, S.; Cardea, S.; Vitillo, J. G.; Guerra, G. *RSC Advances* 2012, *2*, 12011.

(16) Guerra, G.; De Rosa, C.; Petraccone, V.; Corradini, P.; Vitagliano, V. M. *Macromolecules* 1990, *23*, 1539.

(17) Rizzo, P.; Daniel, C.; De Girolamo Del Mauro, A.; Guerra, G. *Chem. Mater.* 2007, *19*, 3864.

(18) Rizzo, P.; Sanguigno, L.; Venditto, V.; Guerra, G. *Sensors (Peterborough, NH)* 2009, 9816.

(19) Petraccone, V.; Ballesteros, O. R. D.; Tarallo, O.; Rizzo, P. *Chem. Mater.* 2008, *20*, 3663.

(20) De Rosa, C.; Guerra, G.; Petraccone, V.; Pirozzi, B. *Macromolecules* 1997, *30*, 4147.

(21) Albunia, A. R.; Rizzo, P.; Guerra, G. *Chem. Mater.* 2009, *21*, 3370.

(22) Tarallo, O.; Petraccone, V. *Macromolecular Chemistry and Physics* 2004, *205*, 1351.

(23) Petraccone, V.; Tarallo, O.; Venditto, V.; Guerra, G. *Macromolecules* 2005, *38*, 6965.

(24) Malik, S.; Rochas, C.; Guenet, J. M. *Macromolecules* 2006, *39*, 1000.

(25) Pierre, A. C.; Rigacci, A. In *Aerogels Handbook*; Aegerter, M. A., Leventis, N., Koebel, M. M., Eds.; Springer 2011, p 21.

(26) Guerra, G.; Mensitieri, G.; Venditto, V.; Reverchon, E.; Daniel, C.; Int. Appl. WO2005012402A1: 2005.

(27) Daniel, C.; Alfano, D.; Guerra, G. *Macromolecules* 2003, *36*, 1713.

(28) Daniel, C.; Alfano, D.; Venditto, V.; Cardea, S.; Reverchon, E.; Larobina, D.; Mensitieri, G.; Guerra, G. *Advanced Materials* 2005, *17*, 1515.

(29) Quignard, F.; Valentin, R.; Di Renzo, F. *New Journal of Chemistry* 2008, *32*, 1300.

(30) García-González, C. a.; Alnaief, M.; Smirnova, I. *Carbohydrate Polymers* 2011, *86*, 1425.

(31) Daniel, C.; Montefusco, T.; Rizzo, P.; Musto, P.; Guerra, G. *Polymer* 2010, *51*, 4599.

(32) Loria, M.; Vaiano, V.; Sannino, D.; Venditto, V. *In preparation* 2013.

(33) Daniel, C.; Giudice, S.; Guerra, G. *Chem. Mater.* 2009, *21*, 1028.

(34) Borriello, A.; Agoretti, P.; Ambrosio, L.; Fasano, G.; Pellegrino, M.; Venditto, V.; Guerra, G. *Chem. Mater.* 2009, *21*, 3191.

(35) The experimental apparatus is a homemade system realized by Prof. Sannino and Dr. Vaiano of the INSTM unit at the Department of Industrial Engineering of University of Salerno.

(36) 5 ppm is the lowest concentration that we can test due to the MS sensitivity limit, which is 2 ppm.

(37) Crank, J. *THE MATHEMATICS OF DIFFUSION*; Clarendon Press, Oxford, 1975.

(38) Loria, M.; Venditto, V.; Vaiano, V.; Sannino, D.; Ciambelli, P.; Secchi, A. In *Frontiers in Polymer Science* Sitges, Spain, 2013, p P1.161.

(39) Webber, M. E.; Pushkarsky, M.; Patel, C. K. N. *Journal of Applied Physics* 2005, *97*, 113101.

(40) Annunziata, L.; Albunia, A. R.; Venditto, V.; Mensitieri, G.; Guerra, G. *Macromolecules* 2006, *39*, 9166.

(41) Albunia, A. R.; Venditto, V.; Guerra, G. *Journal*

of Polymer Science Part B: Polymer Physics 2012, *50*, 1474.

(42) Loria, M.; Venditto, V.; Guerra, G. In *EPF* Pisa, Italy, 2013, p P2.98.

(43) Albunia, A. R.; Musto, P.; Guerra, G. *Polymer* 2006, *47*, 234.

(44) Guerra, G.; Manfredi, C.; Musto, P.; Tavone, S. *Macromolecules* 1998, *31*, 1329.

(45) Hermans, P. H.; Weidinger, A. *Journal of Applied Physics* 1948, *19*, 491.

(46) http://www.eng.auburn.edu.